Article

Establishment of salivary tissue-organoid biorepository: characterizing salivary gland stem/progenitor cells and novel differentiation marker PSMA/FOLH1

Check for updates

Syed Mohammed Musheer Aalam [1,11], Ana Rita Varela[1,11], Aalim Khaderi[1,11], Ronsard J. Mondesir[1,11], Dong-Gi Mun[1,11], Andrew Ding [1,10], Isabelle M. A. Lombaert [2,3], Rob P. Coppes [4], Chitra Priya Emperumal[1], Akhilesh Pandey[1,5,6,12], Jeffrey R. Janus[7,8,12] ✉ & Nagarajan Kannan [1,8,9,12] ✉

The salivary gland (SG) is vital for oral function and overall health through secretion of saliva. However salivary dysfunction due to aging, medications, autoimmune disorders, and cancer treatments poses significant challenges. We established the first diverse and clinically annotated salivary regenerative biobank at Mayo Clinic to study salivary gland stem/progenitor cells (SGSPCs). Optimization of cell isolation and progenitor assays revealed SGSPCs enriched within the CD24/EpCAM/CD49f+ and PSMA- phenotypes of both submandibular and parotid glands, with clonal differentiation assays highlighting heterogeneity. Induction of PSMA/FOLH1 expression was associated with SGSPC differentiation. Using mass spectrometry-based single cell proteomics, we identified 2461 proteins in SGSPC-enriched cells, including co-expressed cytokeratins, expressed in rare salivary ductal basal cells. Additionally, PRDX, a unique class of peroxiredoxin peroxidases enriched in SGSPCs, demonstrated H_2O_2-dependent growth, suggesting a role in salivary homeostasis. These findings provide a foundation for SGSPC research and potential regenerative therapies for salivary gland dysfunction.

The major salivary glands (SG), namely parotid (PG), sub-mandibular (SMG), and sublingual, play an important role in oral health. These glands comprise multiple epithelial cell types contributing to the dynamic composition of saliva[1]. The watery secretion of PG, the mucous richness of sublingual, and the versatile watery/mucous mix of SMG highlight their unique contribution to an individual's quality of life. Salivary dysfunction leading to xerostomia or hyposalivation (persistent dry mouth due to reduced saliva flow) arises from damage to salivary epithelial cells and/or its microenvironment and a blockade of its normal function resulting in a wide range of health consequences.

Salivary dysfunction increases the risk of dental caries, gum disease, and oral infections (e.g., candidiasis), and halitosis, while impairing fundamental activities like chewing and swallowing, speech and causing discomfort. altered taste, and digestive issues. Given the wide-ranging effects on effects on both oral and overall health, it is important to address salivary dysfunction for improving patients' quality of life and well-being[2].

[1]Department of Laboratory Medicine and Pathology, Mayo Clinic, Rochester, MN, USA. [2]Biologic and Materials Sciences and Prosthodontics, University of Michigan School of Dentistry, 1011 N. University Ave, Ann Arbor, MI, USA. [3]Biointerfaces Institute, University of Michigan, 2900 Plymouth Rd, Ann Arbor, MI, USA. [4]Departments of Radiation Oncology and Biomedical Sciences, University of Groningen, University Medical Center Groningen, Groningen, The Netherlands. [5]Center for Individualized Medicine, Mayo Clinic, Rochester, MN, USA. [6]Manipal Academy of Higher Education, Manipal, Karnataka, India. [7]Department of Otolaryngology-Head and Neck Surgery, Mayo Clinic, Jacksonville, FL, USA. [8]Center for Regenerative Biotherapeutics, Mayo Clinic, Rochester, MN, USA. [9]Mayo Clinic Comprehensive Cancer Center, Mayo Clinic, Rochester, MN, USA. [10]Present address: Department of Biological Engineering, Massachusetts Institute of Technology, Cambridge, MA, USA. [11]These authors contributed equally: Syed Mohammed Musheer Aalam, Ana Rita Varela, Aalim Khaderi, Ronsard J. Mondesir, Dong-Gi Mun. [12]These authors jointly supervised this work: Akhilesh Pandey, Jeffrey R. Janus, Nagarajan Kannan. ✉e-mail: Janus.Jeffrey@mayo.edu; Kannan.Nagarajan@mayo.edu

Salivary dysfunction can result from conditions, including autoimmune disorders like Sjögren's Syndrome, rheumatoid arthritis, and systemic lupus erythematosus, cancer treatments like head and neck radiation therapy[3], Prostate Specific Membrane Antigen (PSMA)-targeted radionuclide therapy[4] and immunotherapies[5], and certain medications. Other contributing factors include diabetes, viral infections (mumps, human immuno-deficiency virus, hepatitis), aging, trauma, surgery-related nerve damage, dehydration, and salivary gland tumors. Despite decades of research in salivary gland function using animal models[6], a curative treatment for salivary dysfunction remains elusive[7].

Emerging studies focus on leveraging stem cells (SC) and tissue engineering approaches to regenerate damaged or irradiated salivary glands. Transplantable cells capable of restoring saliva function have been identified in recent years, paving the way for regenerative therapies[8–10]. These approaches aim to address the consequences of salivary dysfunction, such as xerostomia, by promoting the repair and restoration of functional salivary tissues, but lack of community accessible clinically annotated salivary specimen suitable for SC investigation, which is a major impediment to development of salivary regenerative medicine. To address this gap, we have established a salivary regenerative biobank at the Mayo Clinic from patients undergoing head and surgery as well as from autopsies and clinical data and from individuals contributing to our biobank.

The stemness, plasticity and transplantability of salivary cells are not well understood. Studies in exocrine mammary gland with similar epithelial structures suggest that non-transplantable differentiated myoepithelial and luminal cells following short-term in vitro culture or genetic manipulation exhibit stemness, displaying both transplantability and lineage regeneration[11–13]. Studies in mouse salivary glands indicate the heightened proliferation potential of lineage-committed differentiated cells, such as acinar cells[14], and upon radiation injury, various ductal progenitor cells play a role in maintaining tissue homeostasis[15]. Therefore, human specimen resources and protocols to investigate these diverse salivary cell types and their regenerative activities and transplantabilities are essential to develop salivary regenerative medicine. Herein, we describe an optimal protocol to isolate, expand, and quantitatively investigate salivary cell immunophenotypes and growth properties in both 2D and 3D-matrigel assays. We developed rigorous methods to isolate salivary gland stem and progenitor cells (SGSPC) by flow cytometry using CD24/CD49f/EpCAM+ and PSMA- phenotypes. We further generated the first known single-cell proteomic map of 271 SGSPC-enriched EpCAM+ cells from PG and SMG using mass spectrometry. This single-cell proteomic map identified distinct protein co-expression of keratins, which are found in rare, scattered salivary gland basal duct cells suggesting their potential role as the tissue origin of SGSPC. Our unique tissue-organoid biobank and novel quantitative approach to study SGSPC provide a robust framework for advancing personalized regenerative medicine research targeting salivary gland dysfunction.

Results
Establishment of a comprehensive living salivary tissue-organoid biobank
Herein, we utilized previously established method from living mammary tissue-organoid biobanking for stem and progenitor cell investigation[16–30], to establish clinically annotated salivary biobanking protocol involving salivary gland tissue. Surgical resections of SMG and PG glands were performed on consenting patients aged 18 and older undergoing head and neck surgery at Mayo Clinic Jacksonville. Tissue samples from deceased individuals were obtained during autopsies at Mayo Clinic Rochester. In brief, each specimen received in the laboratory, was weighed and manually minced (mechanically) into fine pieces and subsequently subjected to gradual enzymatic dissociation with collagenase and hyaluronidase. The resulting epithelial enriched 2–4 mm salivary tissue fragments (referred to as 'salivary tissue-organoids') were cryopreserved in basal media containing serum and DMSO (see Methods). For each specimen, the biobank also generates two tissue fragments: one snap-frozen tissue and another for formalin-fixed

paraffin-embedded block preparation; and all specimens were annotated, tracked and stored using the Mayo Clinic's Research Laboratory Information Management System (RLIMS), a web-based application available at all Mayo locations. (Fig. 1A). Quality control assessments for the cryopreserved salivary organoids are performed to evaluate cell viability (Supplementary Fig. S1A, B), microbial contamination and epithelial content by FACS. Any signs of microbial contamination were documented.

In total of 304 specimens were collected from 208 donors, with 45.7% obtained from female individuals representing diverse age, race, ethnicity, medical history, various exposures and mortality status, all of which contributed to the biobank (Table 1, and Fig. 1B–E). We generated 2044 tissue-organoid cryovials including 1148 from male and 896 from female donors. Organ-related issues were the primary cause of death (40.2%), followed by cardiovascular conditions (32.0%). Notably, 14.9% were current smokers, and 38.0% were former smokers. Various chronic conditions, such as cancer, head and neck radiotherapy, and chemotherapy treatment, were prevalent among donors. The biobank included samples from patients with salivary gland neoplasms, diabetes mellitus, and other conditions including Sjögren's disease. A significant portion had a history of COVID-19 (for details refer to Table 1).

The hematoxylin and eosin (H&E) staining reveals a level of disorganization in the cryopreserved tissue-organoids compared to intact salivary gland tissue sections (Fig. 1F). This could be the result of the mechanical and enzymatic dissociation process used to prepare the organoids. Specifically, the use of enzymes such as collagenase and hyaluronidase during tissue dissociation helps to remove stromal and fat tissues, resulting in enrichment of epithelial tissues. These tissue-organoids were subsequently dissociated into single cells and were evaluated for the presence of primitive cells with proliferative activity using 2D culture and 3D-matrigel organoid culture system that supported clonal development (see Methods). In particular, single cell-derived organoids have emerged as systems to approximate progenitor activity in vitro in many tissue types[31] including SG[8] and represent a valuable tool to evaluate the developmental activities of salivary cells[32].

In 2D cultures, the majority of cells exhibited a typical epithelial morphology (Fig. 1G). In 3D Matrigel organoid cultures, we observed heterogeneous morphologies (Fig. 1H), including solid structures with branching and budding features, as well as organoids with cystic appearances. These observations are consistent with previous studies on salivary and other exocrine tissues, suggesting a luminal origin for cystic organoids and a basal origin for solid organoids[21,33]. Additionally, these 3D organoids expressed acinar and ductal differentiation markers, supporting their epithelial lineage (Fig. 1I, J). Using the 3D-matrigel organoid-initiating cell (3D OIC) assay system the frequency of SGSPCs was estimated to be ~1 in 1700 isolated single cells from cryopreserved salivary tissue-organoids (Fig. 1K). This comprehensive biobanking protocol establishes a valuable resource for advancing research in salivary regenerative medicine. For details on accessing biobank specimens and data, kindly refer to the Methods section.

Immunophenotyping reveals rapid selection of salivary epithelial cells in vitro
We next employed FACS to immunophenotype cells. Hereto, we conducted an in-depth analysis of epithelial biomarker expression in single cells obtained from freshly dissociated PG and SMG tissue-organoids. Additionally, we examined cells from 2D cultured derivatives across various passages in media-1 and media-2. Using cell surface markers reported in the literature and human protein atlas, we developed an antibody cocktail targeting endothelial CD31, hematopoietic CD45, stromal CD34, epithelial markers EpCAM, CD24, and CD49f, and *FOLH1*-encoded prostate specific membrane antigen (PSMA), somatostatin receptor (SSTR)2, and DAPI. We performed FACS, depleting endothelial, hematopoietic, and dead cells, and subsequently gated viable cells for epithelial biomarker expression[8,18,34–38] (Fig. 2A).

The cell surface epithelial marker expression profiles of freshly dissociated salivary tissue-organoids (CD49f: SMG = 23.58%, PG = 16.48%;
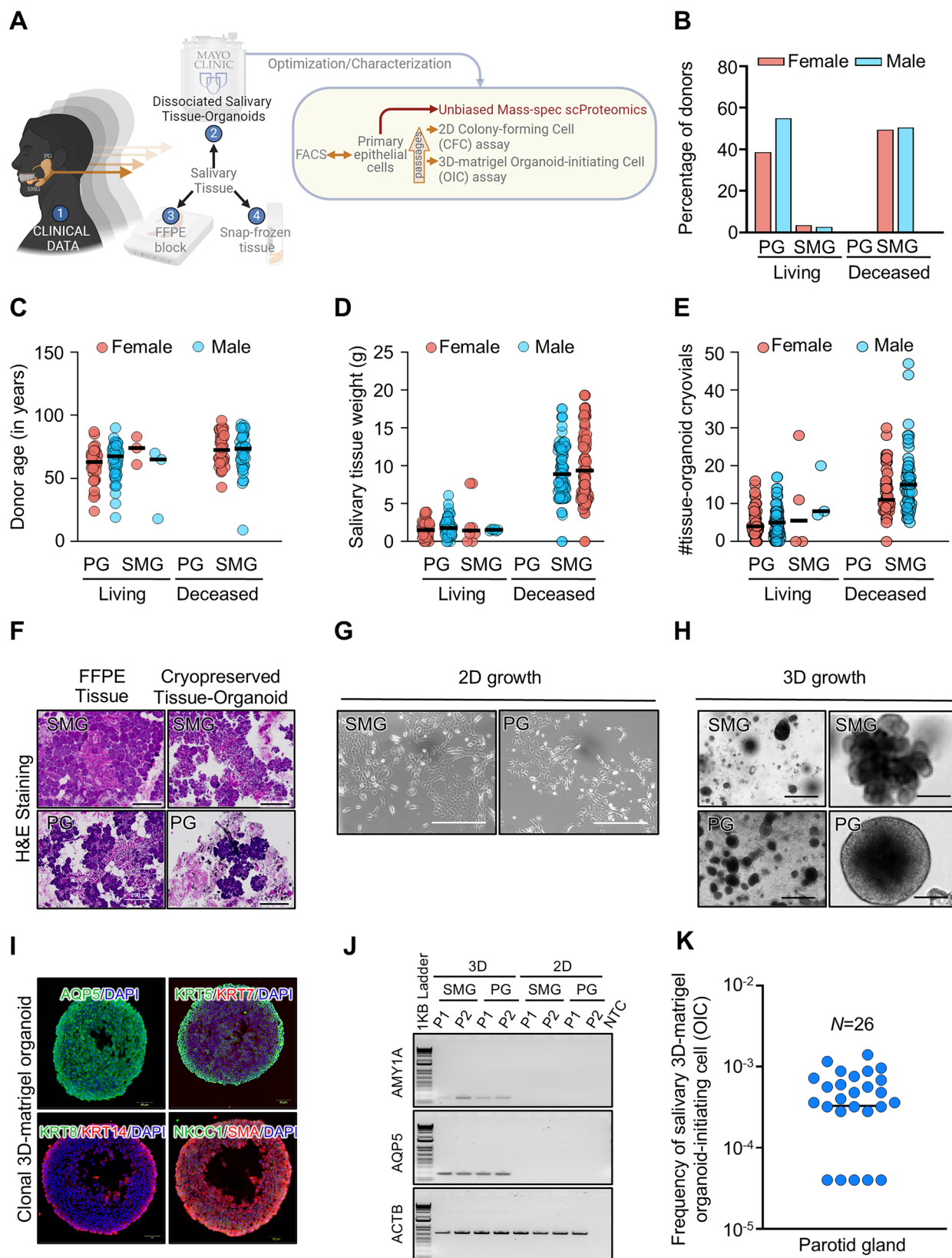
CD24: SMG = 10.68%, PG = 16.48%; EpCAM: SMG = 6.84%, PG = 2.37%; PSMA: SMG = 1.38%, PG = 2.87%, SSTR2: SMG = 0.28%, PG = 0.29%) were not significantly different suggesting that the dissociation protocol enabled purification of primary salivary epithelial cells with shared immunophenotypes in the two major salivary gland (Fig. 2B). The expression of

these markers remained consistent between genders (Supplementary Fig. S2).

In 2D culture, salivary cells from SMG and PG exhibited robust expansion for up to four passages. FACS based co-expression analysis across passage (P)1 to P4 demonstrated ~90% cells expressing epithelial markers

Fig. 1 | Salivary tissue-organoid biobanking preserves primitive salivary cells. **A** Schematic workflow outlining the steps involved in the processing of PG and SMG tissues to generate tissue-organoids, as well as their cryopreservation and biobanking from living or deceased male and female donors (created using Biorender.com). **B** Plot showing the age distribution among PG and SMG donors, considering both living and deceased individuals of both genders in the biobank. **C**) Plot depicting the weight distribution of PG and SMG tissues received at the laboratory, considering both living and deceased donors of both genders. **D** Plot illustrating the quantity of patient-derived tissue-organoid cryovials obtained from PG and SMG tissue masses received at the laboratory, considering both living and deceased donors of both genders. **E** Bar plot illustrating the distribution of PG and SMG tissue-organoids in the biobank, considering donors from both living and deceased individuals of both genders. **F** H&E staining of SMG and PG tissues and their corresponding tissue-organoids show characteristic ductal and acinar structures (100x magnification). **G** Representative brightfield images of cultured SMG and PG cells isolated from respective cryopreserved tissue-organoids (100x magnification). **H** Representative brightfield images of SMG and PG organoids cultured in 3D-matrigel (40x and 100x magnification) derived in culture following dissociation of respective tissue-organoids. **I** Representative immunofluorescence staining of 3D-matrigel-derived PG organoids with DAPI, Aquaporin 5, NKCC1, SMA, KRT5, KRT7, KRT8 and KRT14 antibodies. **J** Agarose gel (2%) image showing expression of *AMY1A* (162 bp), *AQP5* (178 bp) in two consecutive 3D organoid cultures but not in 2D SMG and PG cultures by Reverse Transcriptase-Polymerase Chain Reaction (RT-PCR). Gene expression was normalized to *ACTB* (494 bp). Uncropped gel images are supplied as Supplementary Fig. S12. K) Plot showing 3D OIC frequency from cryopreserved salivary gland tissue-organoids.

CD24, CD49f and EpCAM, and lacking expression of PSMA (~ 5%) and SSTR2 (<1%) across PG and SMG cultures. Hematopoietic (CD45 +) and non-epithelial stromal (CD31/CD34 +) cells were found to be poorly detected in cultured cells, indicating rapid selection for epithelial cells under these conditions (Fig. 2C). Notably, an initial increase in PSMA+ cells was observed in culture, reaching approximately 10% at passage 2 before declining in subsequent passages. SSTR2 expression remained consistently low throughout the culture period, suggesting enrichment of a subset of cells likely to be ductal in origin (Fig. 2C, D and Supplementary Fig. S3-S4A–C). Consistent with our FACS analysis, cells in media-1 and media-2, maintained their characteristic epithelial morphology and expression of epithelial markers as shown by E-cadherin immunofluorescence throughout the culture period (Fig. 2E–G, Supplementary Fig. S4D, E). It is worth noting that majority of cultures reached passage 3 by three weeks. Taken together, this comprehensive flow cytometry analysis provides insights into the dynamic expression patterns of salivary epithelial biomarkers in cryopreserved tissue-organoids within the biobank and after in vitro expansion, revealing a significant bias toward the selection of ductal epithelial cells.

Functional analysis reveals distinct salivary progenitor populations in vitro

We performed a comprehensive assessment of the cryopreserved tissue-organoids to test the proliferative epithelial cells in 2D culture enriched for SGSPC. We fractionated salivary cells based on CD24, PSMA, EpCAM, and CD49f markers and subjected bulk cells or distinct phenotypic fractions to optimized 2D colony-forming cell (2D CFC) and 3D-matrigel organoid-initiating cell (3D OIC) assays by seeding cell densities that generate clonal outgrowths (see Methods)[21]. To further understand the growth dynamics, we derived primary salivary cells from cyropreserved salivary tissue-organoids and cultured using media-1[39], both with and without fetal calf serum (FCS), or in N2 media[9]. Cultures were conducted in dishes with or without collagen-coated surfaces[17]. Notably, collagen coating had little or no impact on growth in media-1, while cells in N2 media demonstrated sensitivity to collagen coated surfaces (Supplementary Fig. S5A–C). Despite marginal improvements with the inclusion of FCS, we opted for media-1 with FCS and no collagen coating for this study.

The 2D CFC assays revealed three distinct colony morphologies, each representing unique characteristics—spindle (myoepithelial-like), epithelial (ductal-like), and bridge-forming (squamous-like) colonies (Fig. 3A, B). The presence of three distinct clonotypes implies three distinct progenitor origins. The persistence of all clonotypes indicates that these progenitors not only consistently cryopreserved in salivary tissue-organoids but also thrive under in vitro culture conditions. Presence of all three 2D CFC types in FACS-purified cells expressing CD24, EpCAM or CD49f and lack of PSMA and SSTR2 indicated that these distinct progenitor types have common immunophenotypes. A prior study utilizing primary human salivary cells immortalized with origin defective DNA of SV40 has reported similar cellular morphologies in cultures[40].

Furthermore, our investigation revealed detection of up to 18% of 3D-matrigel organoid-initiating cell (OIC) population for PG cells at passage 3.

The average OIC was 3.3% across diverse tissue sources and in vitro culture passages (Fig. 3C and Supplementary Fig. S4C). Notably, the progenitor frequencies observed in the 3D-matrigel OIC assay were consistently higher compared to the 2D colony-forming cell (CFC) assay. Similarly, we detected a maximum of 5% in 2D CFC population within EpCAM+ fraction of PG cells and on average 1.6% across diverse tissue sources and in vitro culture passages (Fig. 3C and Supplementary Fig. S4C).

Interestingly, the lack of distinct growth patterns in 3D organoid cultures (Fig. 3D and Supplementary Fig. S6), compared to the distinct clonotypes observed in 2D CFC assays does not preclude the presence of diverse progenitor populations. Instead, it may suggest that the 3D environment supports a convergent growth pattern[41] or that the phenotypic differences are more subtle and not readily apparent. Additionally, the significant association among salivary gland stem/progenitor cell (SGSPC) markers, including CD24, EpCAM, and CD49f (*p*-value < 0.0001), was evident (Supplementary Fig. S7). In-depth examination of cells derived from 3D-matrigel organoids, as opposed to those expanded in 2D culture, revealed distinct expression patterns of biomarkers, underscoring the intricate and dynamic nature of the differentiation process within the 3D-matrigel environment (Fig. 3E). Additionally, it is noteworthy that the progenitor yield per starting single PG and SMG cell remained comparable over time in culture (Fig. 3F). Together, this implies that the methodologies outlined in this study consistently generate salivary gland stem/progenitor cell numbers, emphasizing the robust selection of the proliferative CD24/EpCAM/CD49f+ SGSPC subset by the specific culture environment.

Induction of PSMA expression during salivary progenitor cell differentiation

The significance of PSMA is underscored by the emergence of PSMA-targeted cancer therapies, which are known to cause salivary dysfunction. Therefore, there is a topical interest in understanding the role of PSMA during salivary development. First, we FACS-purified both PSMA+ and PSMA- cells from bulk cultures (*N* = 15) and assessed their growth properties in 2D CFC and 3D OIC assays (Fig. 4A–C and Supplementary Fig. S6). Notably, a maximum of 2.75% (average 1.15%) and 22% (average 3.74%) of PSMA- cells exhibited robust 2D CFC and 3D OIC activities respectively, while PSMA+ cells were devoid of any growth potential. The PSMA expression is restricted to acinar secretory cells in situ (Fig. 2D). Remarkably, PSMA expression was exclusively localized to the apical membrane of secretory cells within terminal acinar structures, and conspicuously absent from ductal regions (Fig. 2D). Together, these findings imply a plausible hierarchical differentiation model, proposing that PSMA- SGSPC may serve as progenitors for non-cycling (differentiated) PSMA-positive cells with an acinar fate (Fig. 4D). To investigate this hypothesis, PSMA- cells (*N* = 7) were FACS-purified and cultured in 2D or 3D conditions (Fig. 4E–H). Subsequent FACS analysis revealed a gain in PSMA expression in both 2D culture-expanded and 3D-matrigel organoid-derived cells, supporting the notion of PSMA- cells transitioning to a PSMA+ phenotype. Additionally, RT-PCR analysis of 3D organoids (*N* = 2) reveals that the expression of the

## Table 1 | Characteristics of Donors in the Mayo Clinic Salivary Regenerative Biobanking

Characteristics	All Patients N = 208 (100%)	Male N = 113 (100%)	Female N = 95 (100%)
Menopausal Status (Female only)			
Premenopausal	—	—	5 (5.3%)
Perimenopausal	—	—	0 (0.0%)
Postmenopausal	—	—	57 (60.0%)
Unknown	—	—	33 (34.7%)
Pregnancy			
Never	—	—	14 (14.7%)
1–2	—	—	19 (20.0%)
>2	—	—	21 (22.1%)
Unknown	—	—	41 (43.2%)
BMI			
<16	4 (1.9%)	3 (2.6%)	1 (1.1%)
16–25	63 (30.3%)	31 (27.4%)	31 (33.7%)
25–30	56 (26.9%)	35 (31.0%)	21 (22.1%)
>30	76 (36.5%)	39 (34.5%)	37 (38.9%)
Unknown	10 (4.8%)	5 (4.4%)	5 (5.3%)
Race/Ethnicity			
White	185 (88.9%)	101 (89.4%)	84 (88.4%)
Hispanic/Latino	4 (1.9%)	2 (1.8%)	2 (2.1%)
Black/African American	4 (1.9%)	2 (1.8%)	2 (2.1%)
Native American/American Indian	2 (1.0%)	1 (0.9%)	1 (1.05%)
Asian/Pacific Islander	3 (1.4%)	2 (1.8%)	1 (1.05%)
Other	1 (0.5%)	0 (0.0%)	1 (1.05%)
Unknown	9 (4.3%)	5 (4.4%)	4 (4.2%)
Surgery (N = Total Alive)	111	64	47
Unilateral partial parotidectomy	70 (63.1%)	39 (61.0%)	31 (66.0%)
Unilateral total parotidectomy	30 (27.0%)	18 (28.1%)	12 (25.5%)
Unilateral submandibulectomy	8 (7.2%)	5 (7.8%)	3 (6.4%)
Bilateral submandibulectomy	3 (2.7%)	2 (3.1%)	1 (2.1%)
Autopsy (N = Total Deceased)	97	49	48
Bilateral submandibulectomy	93 (95.9%)	49 (100%)	44 (91.7%)
Unilateral submandibulectomy	4 (4.1%)	0 (0.0%)	4 (8.3%)
Cause of Death (N = Total Deceased)	97	49	48
Cardiovascular	31 (32.0%)	16 (32.7%)	15 (31.3%)
Other organs*	39 (40.2%)	17 (34.7%)	22 (45.8%)
Cancer	29 (29.9%)	12 (24.5%)	17 (35.4%)
CNS	24 (24.7%)	16 (32.7%)	8 (16.7%)
Infections (excluding Covid)	14 (14.4%)	5 (10.2%)	9 (18.8%)
Diabetes	16 (16.5%)	9 (18.4%)	7 (14.6%)
Covid	6 (6.2%)	4 (8.2%)	2 (4.2%)
Unknown#	4 (4.1%)	2 (4.1%)	2 (4.2%)
Blunt force injuries	5 (5.2%)	3 (6.1%)	2 (4.2%)
Sialagogue Usage			
Pilocarpine	1 (0.5%)	1 (0.9%)	0 (0.0%)
Cevimeline	0 (0.0%)	0 (0.0%)	0 (0.0%)
No	202 (97.1%)	109 (96.5%)	93 (97.9%)
Unknown	5 (2.4%)	3 (2.7%)	2 (2.1%)
Chronic Diseases			
Rheumatoid arthritis	7 (3.4%)	4 (3.5%)	3 (3.1%)
Sjögren's syndrome	1 (0.48%)	0 (0.0%)	1 (1.05%)
Systemic lupus erythematosus	1 (0.48%)	0 (0.0%)	1 (1.05%)
Amyloidosis	2 (1.0%)	0 (0.0%)	2 (2.1%)

Table 1 (continued) | Characteristics of Donors in the Mayo Clinic Salivary Regenerative Biobanking

Characteristics	All Patients N = 208 (100%)	Male N = 113 (100%)	Female N = 95 (100%)
Primary biliary cirrhosis	5 (2.4%)	3 (2.6%)	2 (2.1%)
Diabetes mellitus	44 (21.3%)	24 (21.3%)	20 (21.0%)
Thyroiditis	1 (0.5%)	0 (0.0%)	2 (2.0%)
None	146 (70.2%)	81 (71.7%)	65 (68.4%)
Unknown	5 (2.4%)	3 (2.6%)	2 (2.1%)
History of Cancer			
Yes	88 (42.3%)	48 (42.5%)	40 (42.1%)
No	115 (55.3%)	62 (54.9%)	53 (55.7%)
Unknown	5 (2.4%)	3 (2.7%)	2 (2.1%)
History of Head & Neck Radiotherapy			
Yes	20 (9.6%)	13 (11.5%)	7 (7.4%)
No	181 (87.0%)	96 (85.0%)	85 (89.5%)
Unknown	7 (3.4%)	4 (3.5%)	3 (3.2%)
History of Chemotherapy			
Yes	34 (16.3%)	18 (15.9%)	16 (16.8%)
No	168 (80.8%)	92 (81.4%)	76 (80.0%)
Unknown	6 (2.9%)	3 (2.7%)	3 (3.2%)
Number of Medications			
None	6 (2.9%)	2 (1.8%)	4 (4.2%)
1-3	28 (13.5%)	17 (15.0%)	11 (11.6%)
4-6	29 (13.9%)	12 (10.6%)	17 (17.9%)
>6	139 (66.8%)	79 (69.9%)	60 (63.2%)
Unknown	6 (2.9%)	3 (2.7%)	3 (3.2%)
Salivary Gland Neoplasm			
Warthin's tumor	3 (1.4%)	3 (2.6%)	0 (0.0%)
Mucoepidermoid carcinoma	1 (0.5%)	0 (0.0%)	1 (1.05%)
None	199 (95.7%)	108 (95.6%)	91 (95.8%)
Unknown	5 (2.4%)	2 (1.8%)	3 (3.2%)
History of Covid-19			
Yes	41 (19.7%)	18 (15.9%)	23 (24.2%)
No	127 (56.9%)	71 (62.9%)	56 (59.0%)
Unknown	40 (19.2%)	24 (21.2%)	16 (16.8%)
Neuropathy			
Parkinson	4 (1.9%)	4 (3.5%)	0 (0.0%)
Alzheimer	6 (2.9%)	4 (3.5%)	2 (2.1%)
Multiple sclerosis	1 (0.5%)	0 (0.0%)	1 (1.05%)
None	193 (92.8%)	103 (91.1%)	90 (94.7%)
Unknown	5 (2.4%)	2 (1.8%)	3 (3.1%)
Chronic Infections			
HCV	2 (1.0%)	1 (0.9%)	1 (1.05%)
HIV	0 (0.0%)	0 (0.0%)	0 (0.0%)
EBV	0 (0.0%)	0 (0.0%)	0 (0.0%)
CMV	0 (0.0%)	0 (0.0%)	0 (0.0%)
None	200 (96.1%)	109 (96.5%)	91 (95.8%)
Unknown	6 (2.9%)	3 (2.6%)	3 (3.2%)
Smoking			
Current	31 (14.9%)	18 (15.9%)	13 (13.7%)
Former	79 (38.0%)	50 (44.2%)	29 (30.5%)
Never	88 (42.3%)	42 (37.2%)	46 (48.4%)
Unknown	10 (4.8%)	3 (2.6%)	7 (7.4%)

*Other organs include Lung, kidney, liver, and pancreas.
#Cause of death unknown at the time of the autopsy
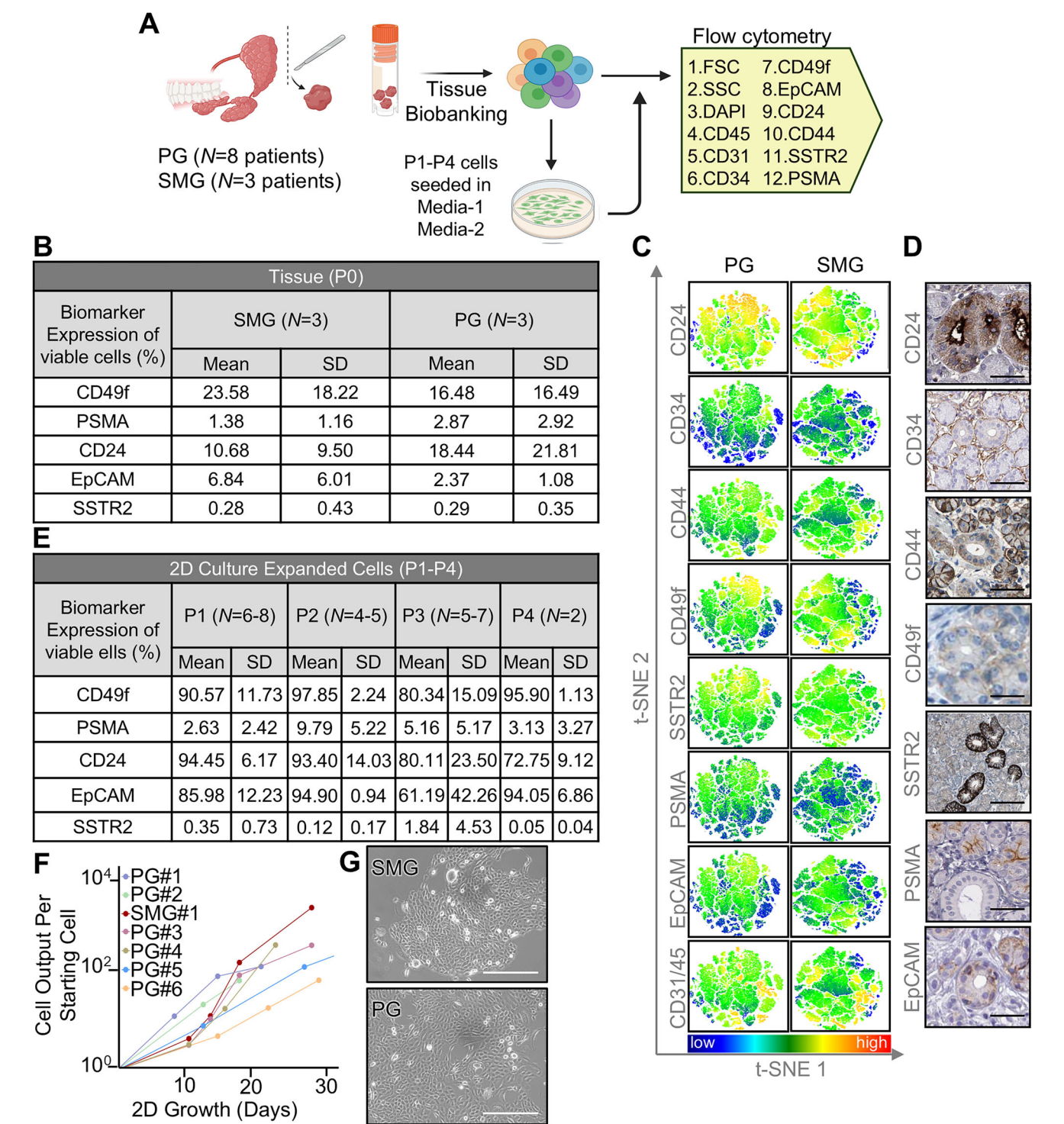
Fig. 2 | Immunophenotypic analysis of salivary tissue-organoids. A Experimental design of FACS-based characterization of cryopreserved salivary gland tissue and culture-expanded salivary cells derived from previously cryopreserved tissue (created using Biorender.com). **B** FACS-based biomarker characterization of unmanipulated salivary gland tissue. **C** T-distributed stochastic neighbor embedding (t-SNE) plots of PG and SMG tissue by biomarker of interest. Coloring correlates with expression intensity. Red indicates high expression, while blue signifies the absence of the cell marker expression. **D** Representative immunohistochemical staining shows expression of various biomarkers in salivary glands (Source: Human Protein Atlas, https://www.proteinatlas.org/). **E** FACS-based biomarker characterization of 2D-culture expanded cells derived from cryopreserved tissue. **F** Salivary cells in culture system can be expanded through four passages. **G** Brightfield image of salivary cell morphology in culture system.

acinar marker AQP5 is limited to PSMA expressing cells (Figs. 1J and 4F). The induction of PSMA expression in cells generated in 2D and 3D-matrigel cultures was observed in all patient samples tested (Supplementary Fig. S8A–C) suggesting spontaneous but poor differentiation in these culture environments.

Gene promoter DNA methylation during cellular differentiation, involving the addition of methyl groups to cytosine nucleotides adjacent to guanines (CpG dinucleotides), is a widespread epigenomic mechanism of gene regulation. A careful examination of the PSMA promoter revealed that it contains a CpG island (Fig. 4H). Thus, we asked whether PSMA is
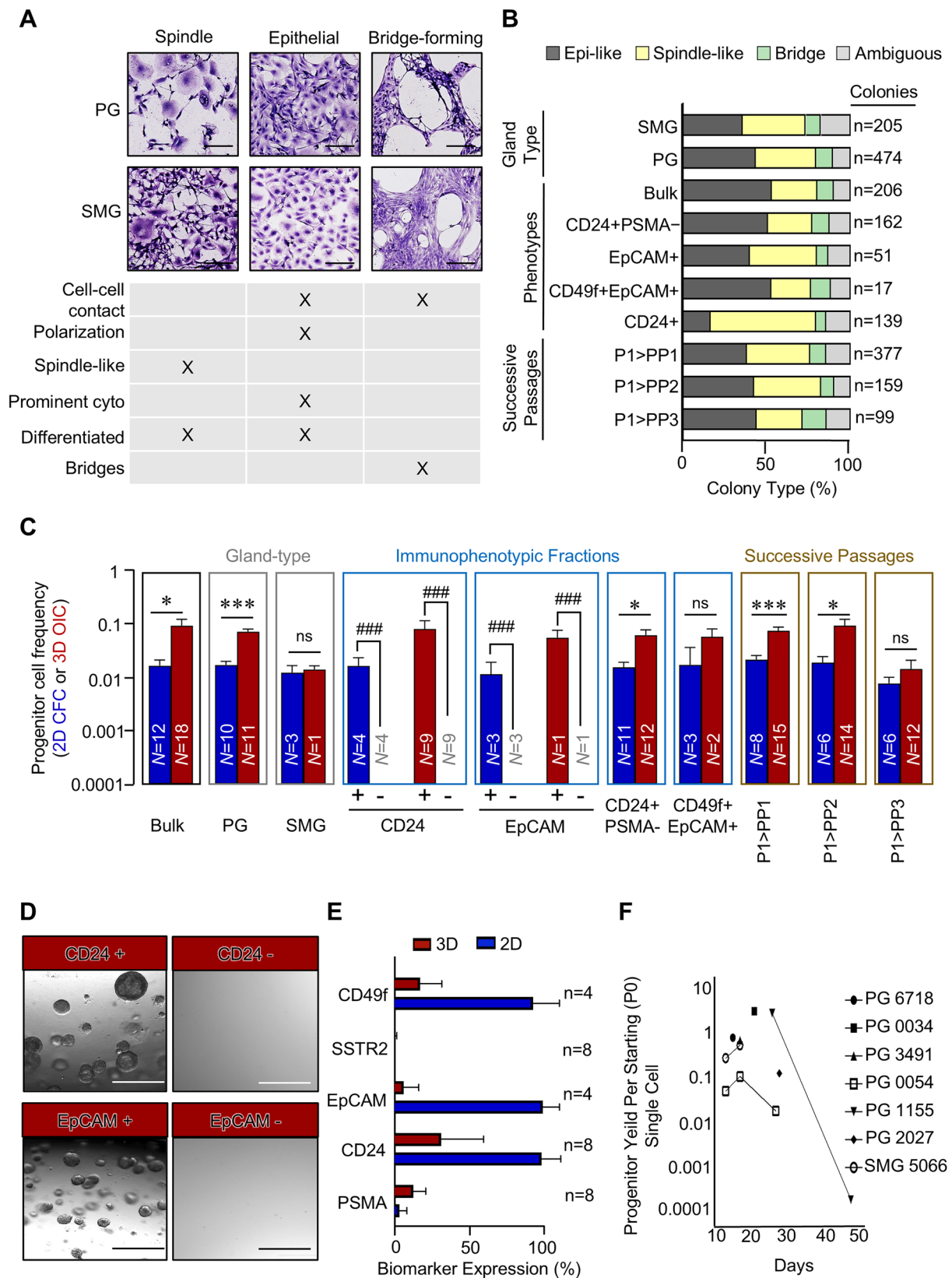
targeted for methylation-mediated silencing in human salivary tissue. We devised a methylation-specific PCR assay to examine PSMA promoter methylation, followed by bisulfite sequencing to validate the hypermethylation of CpG islands within the PSMA promoter in DNA from snap-frozen living SMG tissue (Fig. 4I). Our experiments validated the presence of PSMA promoter hypermethylation in salivary tissue. Our investigation reveals a compelling association between PSMA- primitive salivary cells and the emergence of differentiated PSMA+ salivary acinar secretory cells, suggesting a potential regulatory role for DNA methylation during acinar differentiation.

Fig. 3 | Characterization of salivary progenitor activity in 2D and 3D assays.
A Giemsa staining of salivary colonies obtained in 2D colony-forming cell (CFC) assay showing three distinct morphologies under the microscope. **B** Plot showing the proportions of each of the three distinct colony types in 2D CFC assays when cells are plated, based on salivary gland type, immunophenotype, or in successive passages. **C** Plot showing the frequency of CFC and 3D-matrigel OIC when plated based on salivary gland type, immunophenotype, or in successive passages in the 2D CFC and 3D-matrigel organoid assays. **D** Brightfield microscopy images showing 3D-matrigel organoids obtained from FACS-purified CD24+ and EpCAM+ salivary cells, but not from CD24- and EpCAM- salivary cells. **E** Immunophenotypic characterization of single cells obtained from 3D-matrigel organoids and 2D culture expanded cells from human patient salivary gland tissue-organoids. **F** Plot showing progenitor yield per starting single PG and SMG cell in culture over time. (*, **, and *** indicate *p*-values < 0.05, 0.005, and 0.0005, respectively. #, ##, and ### represent *p*-values < 5×10^{-7}, 5×10^{-10}, and 5×10^{-13}, respectively).

Unbiased mass spectrometry-based single-cell proteomic profiling of primitive salivary cells

To gain molecular insights into SGSPC, we performed proteome profiling of single cells using trapped ion mobility spectrometry (TIMS) in conjunction with a time-of-flight mass spectrometer operated in parallel accumulation-serial fragmentation (PASEF) mode[42,43] (Fig. 5A). To accomplish this, we used our strategy to enrich for progenitors FACS sorting viable (DAPI-) CD45/CD31-EpCAM+ progenitor-enriched cells (referred hereafter as progenitor-enriched single cells) through stringent gating procedures. Subsequently, these single cells were isolated into a 384-well plate and underwent peptide digestion. This approach consistently enabled the detection of ~675 proteins per progenitor-enriched single cell on an average from both PG (*n* = 42, *N* = 1) and SMG (*n* = 29) in the Run1. Following methodological improvements, as described in the previous study[44], Run2 achieved the detection of ~1200 proteins on average per 100 progenitor-enriched cells from each of PG and SMG. Across both runs, no significant difference in the number of proteins detected was observed between PG and SMG cells (Fig. 5B and Supplementary Data 1). Further, about 93.4% and 99.7% of all identified proteins in Run1 and Run2 were highly enriched and shared between both PG and SMG progenitor-enriched single cells (Fig. 5C and Supplementary Fig. S9A, B). Additionally, our analysis identified peptides with post-translational modifications including phosphorylation on serine/threonine/tyrosine (64 sites), lysine methylation (28 sites), di-methylation (16 sites) and tri-methylation (8 sites) (Supplementary Data 2) across both the runs. Further, we also identified top 20 proteins expressed in combined PG and SMG cells as well as those specifically expressed in PG and SMG cells (Fig. 5D and Supplementary Data 3). Subcellular localization of proteins revealed that most of the identified proteins were located in the cytoplasm and nucleus in both SMG and PG cells (Fig. 5E, Supplementary Fig. S9C and Supplementary Data 1). Notably, a significant proportion of these proteins were classified as enzymes, aligning with the characteristic salivary phenotype of the analyzed cells (Fig. 5F, Supplementary Fig. S9D and Supplementary Data 1). Therefore, our findings substantiate the existence of shared protein expression patterns among SGSPC, underscoring a common functional profile for these primitive salivary cells irrespective of origin.

Single-cell proteomics identifies putative origin of primitive salivary cells

Cytokeratins are structural proteins specific to epithelial cells, and their expression patterns can be used to identify and characterize different cell types within epithelial tissues[45]. Therefore, we analyzed PG and SMG single-cell proteomics data to identify cytokeratins distinctly associated with SGSPC. Our comprehensive analysis identified a total of 37 cytokeratins expressed in SMG and PG cells. However, KRT6A, KRT7, KRT8, KRT14, KRT19, KRT23, KRT74 and KRT80 were found to be enriched in PG cells compared to SMG cells (Fig. 6A). We validated expression of these cytokeratins in salivary glands using the human protein atlas and many of these cytokeratins were localized in 'scattered' basal cells within salivary ducts (Fig. 6B, C) with some overlap with myoepithelial cells within salivary acini (Supplementary Fig. S10). Our approach reveals developmental interconnections and proteomic heterogeneity within salivary glands, providing a strong foundation for further study. While the data is strongly indicative of developmental proximity, validation through developmental assays is essential.

We next searched for murine analogs of these human cytokeratins in publicly available single-cell transcriptome databases and consistently found their association with the ductal-basal cell compartment of salivary cells with multiple cytokeratins overlapping with basal/myoepithelial cell clusters providing supplementary evidence supporting their probable development proximity (Fig. 6D, E)[46].

Our findings reveal a remarkably conserved cytokeratin profile in salivary glands across mammalian species, enabling the identification of rare primitive cells. Although comprehensive keratin profiling via single-cell proteomics and scRNA-seq suggests an intricate developmental interconnection among ductal basal and acinar myoepithelial cells, these cells may exhibit niche-specific functions[47]. However, further lineage tracing studies are needed to fully establish the origin of these cells. Moreover, our data suggests that a rare subset of scattered basal cells within ducts, similar to mammary gland, may harbor more primitive functionalities, accessible through our in vitro culture conditions, which are vital for future studies[48].

## Primitive salivary cells display oxidative signaling

To identify differentially expressed proteins, we first performed partial least squares discriminant analysis (PLS-DA), which successfully distinguished PG and SMG cells into separate clusters, suggesting inherent biological divergence between these two cell types (Fig. 7A). Further, variable importance in projection (VIP) of PLS-DA identified proteins that were significantly different between PG and SMG cells. (Fig. 7B). Further, unsupervised hierarchical clustering of the top 50 proteins successfully separated the cells into distinct PG and SMG clusters. However, some PG cells were found to cluster with SMG cells, suggesting potential overlap in protein expression profiles or shared characteristics between these cell types, possibly due to similar functional or molecular properties (Fig. 7C and Supplementary Data 1). Taken together, these observations suggest that protein profiles segregate PG and SMG cells into distinct clusters, while the cells with overlapping profiles are indicative of shared molecular pathways and developmental trajectories between these cells.

Cellular peroxiredoxins (PRDX) are important components of the cellular defense system against oxidative stress, contributing to the maintenance of cellular redox balance and the prevention of oxidative damage[49]. Dysregulation of peroxiredoxins or increased oxidative stress in the SG can potentially contribute to conditions such as inflammation, dry mouth (xerostomia), or other oral health issues[50]. Single-cell proteomics detected several components of the oxidative stress pathway including PRDX1, PRDX4, PRDX3, CAT, and TXN in both PG and SMG cells. Several of these non-glutathione antioxidants were significantly enriched in PG cells compared to SMG cells (Fig. 8A). To functionally validate the role of antioxidant pathways, we treated cultured PG cells (*N* = 3 patients) and SMG cells (*N* = 1 patient) with hydrogen peroxide (H_2O_2) at various concentrations and evaluated their viability by MTT assay. We observed significant increase in MTT absorbance, indicative of enhanced cellular metabolic activity, at H_2O_2 concentrations as high as 50 µM (Fig. 8B) suggesting that oxidative stress levels may stimulate metabolic responses or cell proliferation in salivary gland progenitor cells. To further investigate oxidative stress levels, we performed the CM-H_2DCFDA assay to measure intracellular reactive oxygen species (ROS) generation. We observed a progressive increase in DCF fluorescence intensity of treated cells with increasing H_2O_2 concentrations up to 50 µM, indicating a dose-dependent elevation in ROS production. Taken together, these observations suggest that H_2O_2
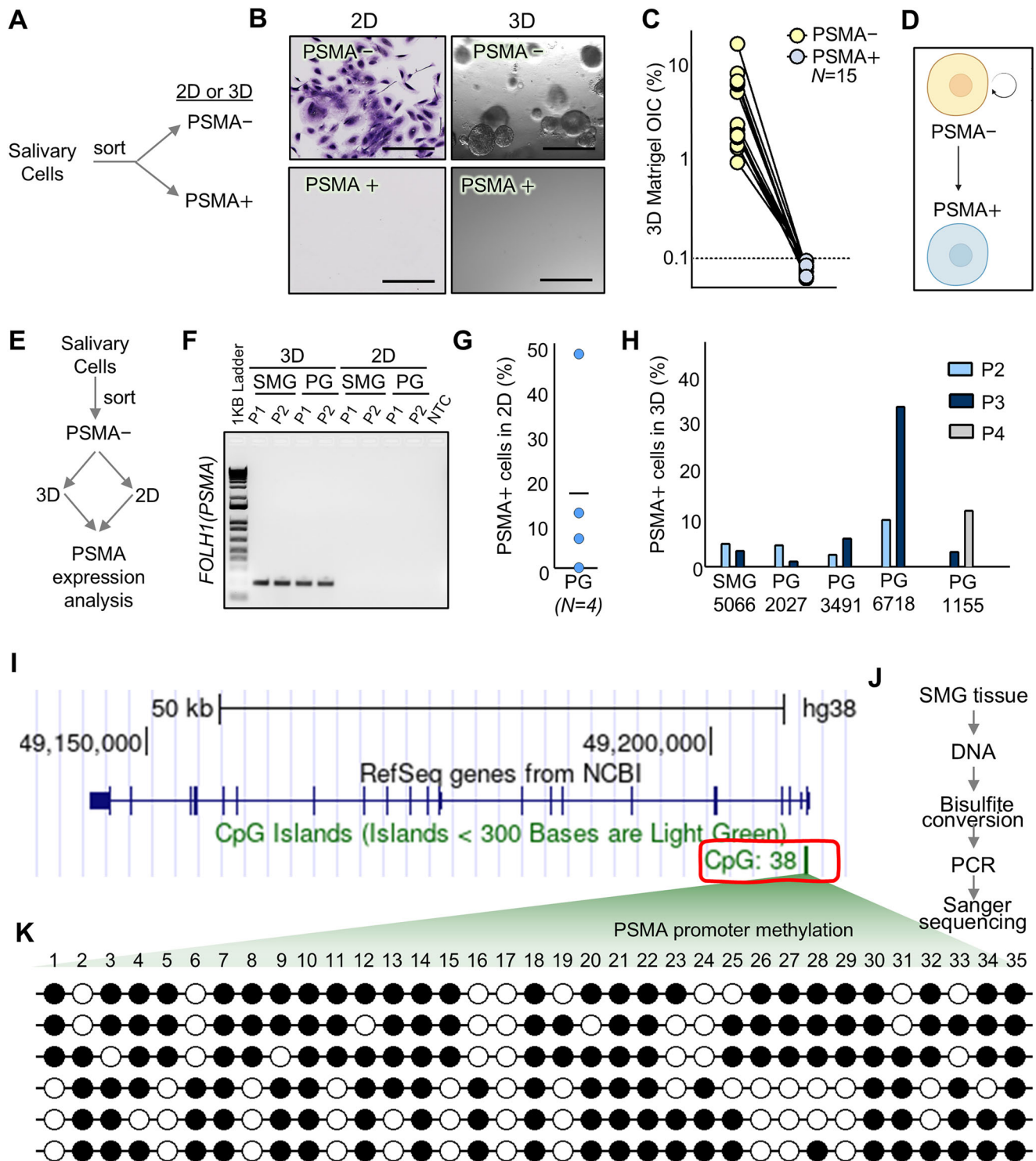
Fig. 4 | PSMA is a SGSPC differentiation marker. A Design of 2D CFC and 3D-matrigel organoid Matrigel experiments to assess clonogenicity of PSMA- and PSMA+ cells. **B** PSMA- cells demonstrate clonogenic capacity in 2D CFC and 3D-matrigel organoid assays, while PSMA+ cells do not. **C** PSMA- cells purified from 15 salivary gland patient samples, unlike PSMA+ purified cells, generate organoids in 3D culture. **D** Proposed hierarchical lineage model by which PSMA+ cells differentiate from the more primitive, stem/progenitor-like, self-renewing PSMA-cells. **E** Experimental design of 2D and 3D FACS-based characterization of growing PSMA- salivary cells to gauge PSMA+ cell generation. **F** Agarose gel (2%) image showing expression of FOLH1(PSMA, 182 bp) in two consecutive 3D organoid cultures but not in 2D SMG and PG cultures by RT-PCR. Uncropped gel images are supplied as Supplementary Fig. S12. **G** PSMA- cells plated in 2D culture generate PSMA+ cells at confluence. **H** 3D-matrigel organoids derived from PSMA- cells give rise to PSMA+ cells through multiple passages. **I** Illustration of CpG islands in human PSMA promoter region. **J** Schematic workflow of bisulfite conversion of 35 of 38 CpG, PCR and sanger sequencing of DNA obtained from SMG. **K** Hypermethylation (~ 70%) of CpG in *PSMA* promoter in SMG tissue. Each circle indicates individual CpG dinucleotides. White and dark circles represent unmethylated and methylated CpG, respectively.
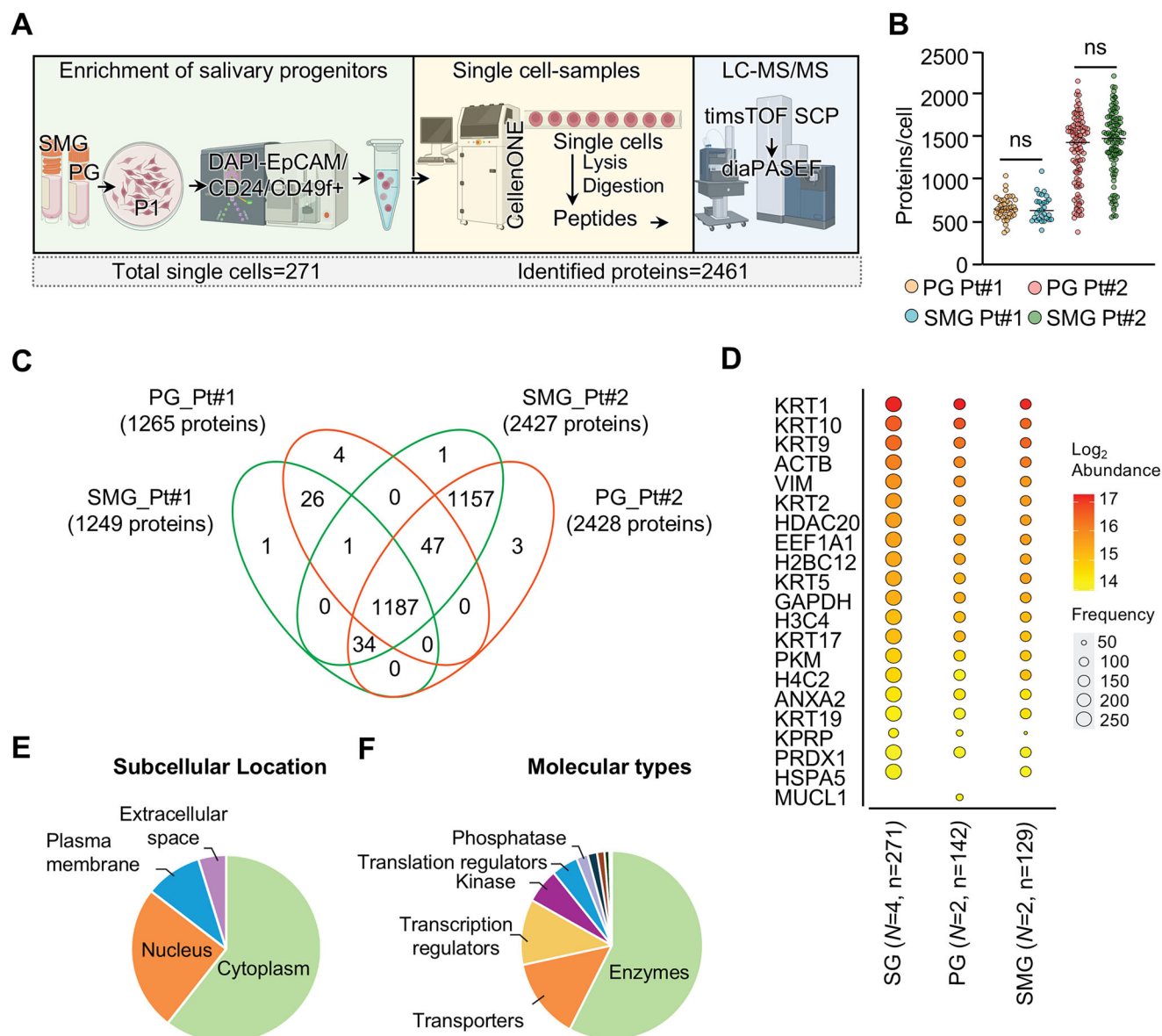
Fig. 5 | Unbiased LC-MS/MS-based single-cell proteomic profiling of purified primitive salivary cells. A Overall workflow for single cell proteomics. Single cells (P1) from PG and SMG cells were isolated by FACS using DAPI-CD45-CD31-EpCAM+ immunophenotype, lysed and digested in 384-well plate using cellenONE platform. Mass spectrometry data of each single cell were acquired in diaPASEF mode using the timsTOF SCP mass spectrometer. A total of 2461 proteins across 271 single cells were identified (created using Biorender.com). **B** Number of identified proteins per cell from SMG and PG P1 cultures. On average, 1143 proteins and 1270 proteins per single cell were identified from PG and SMG, respectively. **C** A Venn diagram showing number of shared and unique differentially expressed proteins within the progenitor-rich single cells of both SMG and PG. **D** Dot plot showing protein counts per cell of 20 most abundantly detected proteins in progenitor rich cells in total salivary gland, SMG and PG. **E** Pie chart showing the subcellular location of proteins detected in PG ($N = 2$, $n = 142$) and SMG cells ($N = 2$, $n = 129$). **G** Pie chart showing the molecular type of proteins detected in PG ($N = 2$, $n = 142$) and SMG cells ($N = 2$, $n = 129$). N represents the number of patient samples and n represents number of SGSPC analyzed. Ingenuity pathway analysis was used for categorizing subcellular localization and function of proteins (QIAGEN Inc., https://digitalinsights.qiagen.com/IPA). N denotes the number of patients; n denotes the number of single cells.

modulates oxidative signaling pathways in SGSPCs, potentially influencing the oxidation of cellular signaling proteins through peroxiredoxins. These findings highlight the adaptive capacity of SGSPCs to moderate oxidative stress and their potential role in redox-mediated cellular processes.

Discussion
We have developed a research protocol for the first clinically annotated salivary gland biobank at the Mayo Clinic to address the current gap in accessible resources for regenerative medicine research in the United States. Notably, our biobank includes PG and SMG samples from both living and deceased donors, providing diversity in terms of age, race, gender, and medical conditions. Our biobank encompasses specimens from various

chronic salivary conditions, including Sjögren's disease, and neoplasms such as mucoepidermoid carcinoma[51,52] and Warthin's tumor[53]. Significantly, our collection includes salivary specimens from patients with a history of COVID-19 infection, that may model and help understand SARS-CoV-2 viral replication in the salivary glands and its potential role in oral transmission and COVID-19-associated xerostomia[32,54,55]. While samples from deceased donors may not fully represent physiological states, they remain an invaluable resource for salivary gland research.

Despite advancements in the understanding of SG development and maintenance, effectively managing SG hypofunction and dysfunction remains a significant clinical challenge. Current treatments are primarily palliative and involve the use of moisturizers such as artificial saliva or saliva
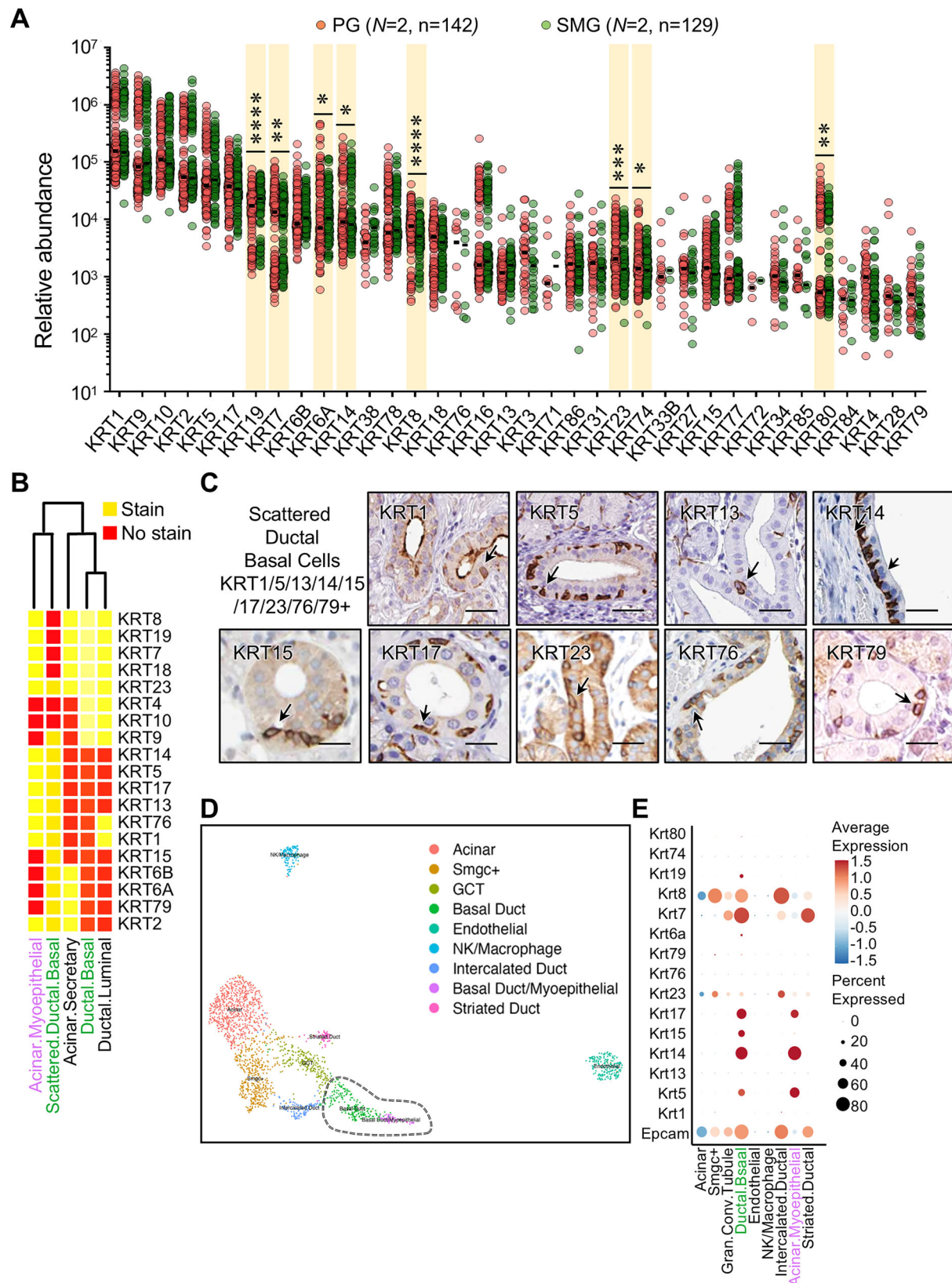
Fig. 6 | Unbiased single cell proteome profiling identifies salivary stem/pro-genitor-specific cytokeratin profile. **A** A plot showing the relative abundance of cytokeratins detected per individual cells (P1) from PG and SMG cells isolated by FACS using DAPI-CD45-CD31-EpCAM+ immunophenotype enriching for SGSPC activity. **B** The relationship between the keratin expression profile identified through single-cell proteomics in SGSPC and the salivary epithelial cell-type specific expression patterns in the immunohistochemistry-based map of human protein expression profiles explored through the Human Protein Atlas (https://www.proteinatlas.org/). **C** SGSPC-expressed keratins map to scattered ductal basal cells in salivary glands (Source: Human Protein Atlas, https://www.proteinatlas.org/). **D** UMAP-based cluster analysis of mouse SMG scRNA-seq data showing salivary cell clusters. **E** Dot plot showing the expression of murine analogs of human SGSPC-expressed cytokeratins (and EpCAM) across mouse salivary cell types (*, ** *** indicate *p*-values < 0.05, 0.005 0.0005, and 0.0001 respectively).
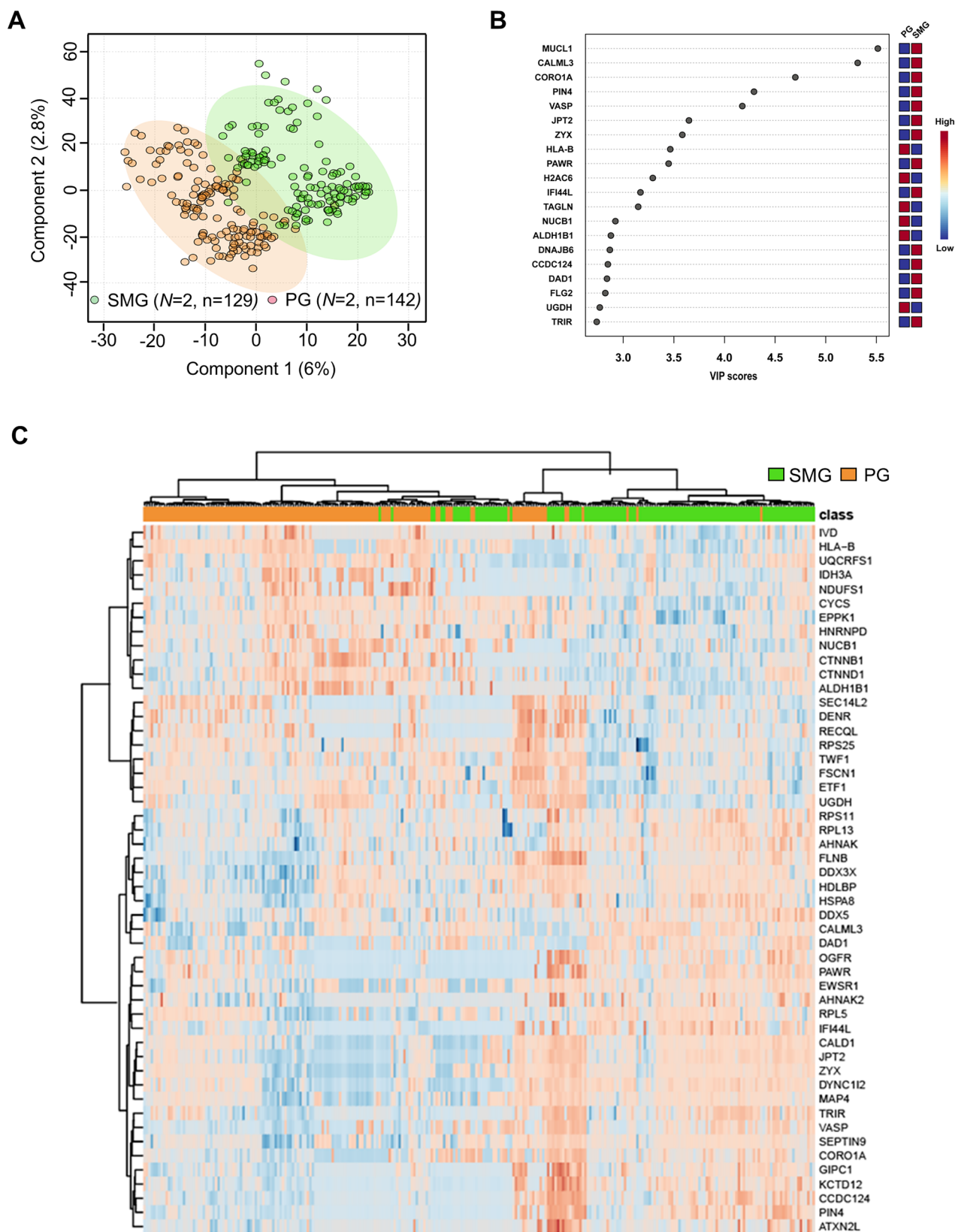
Fig. 7 | Single-cell proteomic analysis discriminates PG and SMG cells. A Partial least squares discriminant analysis (PLS-DA) plot separates PG and SMG cells into distinct clusters. Proteins identified ≥50% of each cell types were used for the analysis after batch effect correction. Each circle represents data from an individual single cell. **B** Variable importance in projection (VIP) score plot of top 15 proteins discriminating PG and SMG cells. **C** Heatmap showing the hierarchical clustering of PG and SMG cells based on their protein expression. Red color represents upregulated and blue color represents down-regulated. The differentially expressed proteins are mentioned on the y-axis, and PG and SMG cells on the x-axis. MetaboAnalyst (https://www.metaboanalyst.ca/docs/About.xhtml) was used to generated PLS-DA plot, VIP score plot and heatmap.
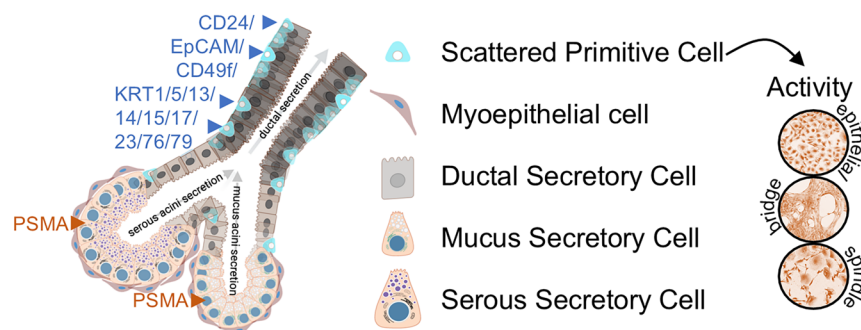
A
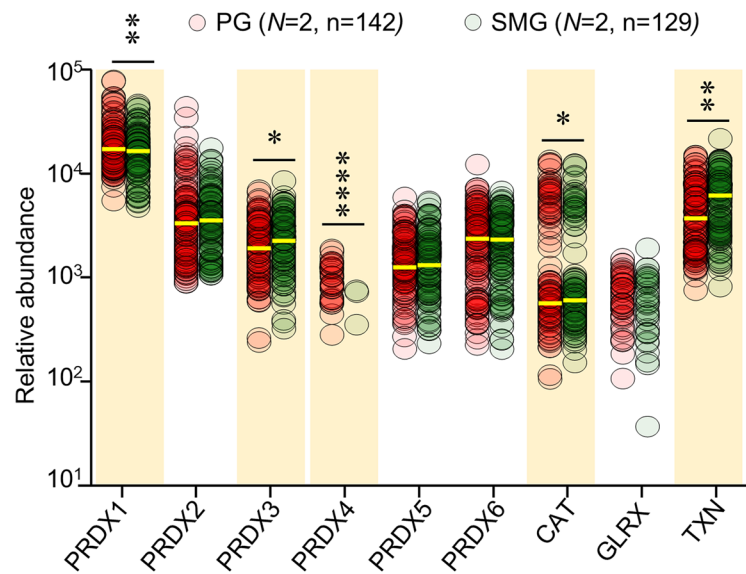
B
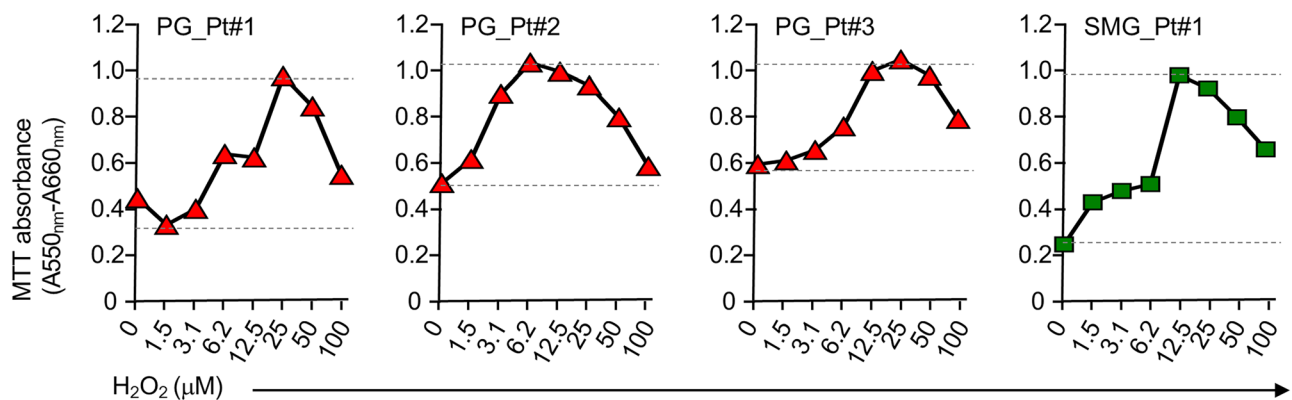
C

Fig. 8 | Single-cell proteomics reveals floodgate oxidative signaling in salivary cells. A Antioxidant enzyme counts per individual cell, illustrating predominantly glutathione-independent peroxiredoxin system in salivary cells. **B** Cellular metabolic activity in proliferative PG (P1, $N = 3$) and SMG (P1, $N = 1$) cells was assessed using the MTT assay, measuring absorbance changes to evaluate cell viability after treatment with varying concentrations of H_2O_2 over a 72 h duration. **C** illustration showing distribution of cell markers and keratins in the salivary glands (created using Biorender.com).

substitutes, as well as systemic medications (e.g., pilocarpine or cevimeline) to stimulate salivary secretion[56] However, these synthetic agents often fall short in adequately compensating for the reduction in saliva production and alleviating associated symptoms, particularly in cases of severe SG damage[57]. Various therapeutic approaches are currently under assessment to address salivary flow restoration in xerostomia patients, with gene therapy being one of them. Ongoing clinical trials are exploring the use of AQP1 gene therapy, employing adeno-associated viruses (AAVs) known for their lower immunogenicity and longer-lasting gene expression compared to adenoviruses[58,59]. However, it is worth noting that tissue damaged by radiation therapy may pose greater challenges for gene therapy, as the fundamental cause of SG dysfunction involves extensive disruption or destruction of the gland at both cellular and extracellular matrix (ECM) levels[60].

Recent clinical observations indicate that irradiated areas containing the highest concentration of SG progenitor cells result in the most substantial reduction in saliva production[61]. These findings suggest that the potential therapeutic approach of SC replacement holds promise for addressing IR-induced xerostomia. One promising avenue of research entails the cultivation of progenitor (or stem) cells in vitro to facilitate the production of SG structures, such as salispheres or organoids. These engineered constructs can then be transplanted or infused into compromised tissue to initiate the development of a new functional gland within its native site[62]. However, despite a substantial body of literature investigating the feasibility of various cell populations for the restoration of SG function, the quest for an abundant and readily accessible source of SG progenitor or stem cells remains ongoing[9,15,62,63]. Nevertheless, a noteworthy development is the first-in-human clinical trial (clinicaltrials.gov identifier: NCT04593589) on autologous SG stem-cell transplantation started in May 2022 undertaken by the University Medical Center Groningen in The Netherlands adding momentum for this research.

While preserving the heterogeneity of the parental tissue, the biobank exhibits enrichment for epithelial cells, thus facilitates the isolation and characterization of transplantable cells with stem/progenitor activity crucial for salivary gland homeostasis. Ongoing studies are exploring these aspects. Viable bulk single cells, purified from cryopreserved specimens, consistently generated organoid structures in matrigel cultures, indicating the presence of cells with primitive activity in our biobanked samples. The lineage hierarchy within SG tissues remains incompletely understood, posing a challenge for the translation and regenerative application of SGSPC[62].

Our identification of markers, including CD24/EpCAM/CD49f as a primitive and PSMA as a differentiation marker, contributes to addressing this gap (Fig. 8C). In fact, CD24 expressing salivary cells have been reported to be enriched with stem and progenitor cell activities, exhibiting self-renewal and multipotent differentiation potential and have the ability to form organoids in vitro, which recapitulate salivary gland architecture[64]. Furthermore, CD24+ cells have been shown to restore salivary gland function in damaged glands in radiation-induced xerostomia mouse models[65,66]. EpCAM is an epithelial cell adhesion molecule, and it has been shown to play an important role in ductal morphogenesis and regeneration in mouse salivary glands[8]. Furthermore, EpCAM+ cells have been extensively studied in other epithelial tissues like the liver, where they mark human hepatic stem/progenitor cells involved in tissue turnover and repair[67]. Similarly, stem cell activity is enriched in EpCAM+ cells of the mammary glands[68]. Notably, recent reports have identified CD49f as a reliable strategy for human SGSPC enrichment by FACS [33; validated in our study (Fig. 2C, D)]. SSTR2 expression is detected in glandular cells of salivary glands[69]. While PSMA is best known for its role in prostate cancer[70], it's expression in salivary glands has been observed primarily in ductal epithelial and endothelial cells[71]. It's folate hydrolase and glutamate carboxypeptidase activities suggest a role in amino acid metabolism and nutrient transport regulation within ductal cells[72]. Additionally, PSMA-expressing ductal cells may play a role in maintaining ductal integrity through cell signaling or cell adhesion mechanisms.

In this study, we generated the first proteomic map at single-cell resolution of SGSPC-enriched cell population. Our analysis revealed common and unique proteins in SMG and PG cells, including KRT5 and KRT14 associated with salivary progenitor cells[73,74]. These keratins serve as essential markers for identifying and isolating stem/progenitor cells in the salivary gland. Notably, KRT5 and KRT19 are recognized progenitor markers in developing salivary glands[75]. KRT14+ progenitor cells are crucial for maintaining ductal homeostasis in submandibular glands[15,76]. Our findings also include KRT7, marking differentiated luminal ductal cells, and KRT76 associated with differentiating layers in stratified epithelia. Understanding these keratins' roles in various tissues indicates their diverse functions, influencing progenitor cells, ductal homeostasis, and differentiation within salivary glands. Similarly, PRDX were among commonly highly upregulated proteins in SGSPC of SMG and PG except for PRDX4, which was almost exclusively expressed in PG suggesting role for these proteins in regulating floodgate oxidative signaling in salivary glands. Our salivary tissue-organoids provide a valuable resource for further exploration of these roles.

We have utilized both SMG and PG samples in most experiments. However, the limited availability of tissue-organoids from living SMG donors restricted our ability to perform analyses directly comparing living SMG and PG tissues in every experiment including CM-H$_2$DCFDA assay. For the scRNA-seq analyses, data from mouse SMG tissues were included, while data from mouse PG cells were not available due to the lack of high-quality scRNA-seq datasets for mouse PG in public databases. This limitation highlights an unmet need for comprehensive molecular datasets for PG cells. Future efforts will focus on generating and publishing scRNA-seq data for PG to support more detailed analyses of these cell types.

It is noteworthy that our biobank offers a diverse range of salivary gland organoid samples, but it predominantly represents white and aged individuals, reflecting the demographic distribution of the population sampled. We have reported this demographic limitation in Table 1 and it may affect the generalizability of our findings to other populations. However, the standardized protocols and robust analytical approaches employed ensure that the biobank remains a valuable resource for salivary gland research. Additionally, we collected samples from donors with wide range of health conditions, including samples from individuals with a history of COVID-19. While we did not analyze this variable in the current study, it underscores the potential for future investigations of how specific health conditions might influence salivary gland biology. We acknowledge these demographic limitations and are actively working to increase diversity in future collections.

In summary, the Mayo Clinic's salivary tissue-organoid biobanking and research approach to investigate SGSPC, combined with their proteomic maps, represent a novel resource for salivary regeneration research.

Methods
Donor eligibility, informed consent process, specimen collection sites and access
The Mayo Clinic Salivary Tissue-Organoid Biobank (referred to as biobank) is an opt-in biobank for which written informed consent was obtained from the participants. The informed consent was reviewed and approved by the Mayo Institutional Review Board to ensure that the consenting process meets all ethical and legal requirements (IRB#17-003710 and 20-002773). Biobank participants agreed to permit the use of samples and/or data from multiple studies, provide access to questionnaires and data from the medical record (including past, present and future details). Moreover, for the biobank, participants allowed access to stored clinical samples, and permit the sharing of deidentified data with other researchers. Participants were not contacted for additional studies. The consent document discusses privacy protections and risks involved in participation in the study. Further, the consent discusses the potential for receiving results from projects that use the sbiobank as a resource. It also provides 2 check boxes (included at the suggestion of the community members), allowing the participant the options of (1) not allowing access to stored clinical specimens for research and (2) not allowing family members access to samples after their death.

Patients at Mayo Clinic who are 18 years or older, who can communicate in English or use interpreters if needed, and are able to consent, were enrolled in the biobank. Study materials were provided in English only. Recruitment to the biobank was primarily conducted in person for prospective participants scheduled for a pre-surgical appointment at The Department of Otorhinolaryngology, Mayo Clinic, Jacksonville, Florida. The enrollment started at Mayo Clinic Jacksonville in September 2020 with active ongoing collections. All experiments and procedures involving human participants were conducted in accordance with relevant ethical regulations, including the Declaration of Helsinki.

All requests for specimens and data will be thoroughly reviewed in accordance with institutional policy and alignment with collaborative goals to advance salivary gland regeneration research. For further details, please email corresponding authors.

Viable salivary specimen processing, quality control and derivatives

Tumor-free clinical residual SG specimens from living donors were obtained from the anatomic pathology laboratory at Mayo Clinic Jacksonville, and SMG tissue from deceased donors is obtained from the autopsy laboratory at Mayo Clinic Rochester. The specimen from living donor was collected in a buffered media containing DMEM (Corning), 5% FCS (Gibco), and 1x penicillin-streptomycin (Gibco) and transported overnight on ice (FedEx) to the Stem and Cancer Biology Laboratory at Mayo Clinic Rochester for further processing and biobanking. Specimens were processed using the mechanical and enzymatic dissociation method. Specimens were finely minced using sterile blades and transferred into conical, ridged Erlenmeyer flask and dissociated overnight (~ 16-18 hours) in DMEM F-12 (Ham's, Gibco) supplemented with 2% wt/vol BSA (Fraction V; Life Technologies), 300 U/mL collagenase (Sigma-Aldrich), and 100 U/mL hyaluronidase (Sigma-Aldrich, Supplementary Table S1) at 80 rpm, 37 °C and 5% CO_2. Enough dissociation media was added to immerse the tissue (4 ml dissociation media per 1 g of tissue). Subsequently, the material was transferred to a 50 ml conical centrifuge tube, the flask was washed with warm DMEM F-12 and added to the centrifuge tube. Further, tubes were centrifuged at $100 \times g$ for 5 min and supernatant was discarded. The tissue pellet was highly enriched in epithelial organoids and was resuspended in freezing media containing 50% DMEM (Corning), 44% FCS (Gibco), and 6% DMSO (Invitrogen). The tissue-organoids were then divided into appropriate number of aliquots based on its size. The tissue-organoid aliquots were frozen in −80 °C in a freezing container (Thermo Scientific™ Mr. Frosty™ Freezing Container) and transferred next day to temperature monitored cryostorage tanks supported by Mayo Clinic's Center for Regenerative Biotherapeutics (CRB).

Each tissue-organoid cryovial was barcoded with sample attributes and are assigned storage using RLIMS (Research Laboratory Information Management System). RLIMS is a web-based application utilized by Mayo Clinic research laboratories to create, annotate, and track samples. Moreover, RLIMS can seamlessly integrate with laboratory sample processing, storing, and delivering structured data on samples. Further, for each specimen, a fraction of tissue-organoids was dropped into basal media and tested for microbial contamination for 7 days at 37 °C and 5% CO_2 and results were recorded.

Microscopy

Organoids were then stained as previously described[6] with primary and secondary antibodies described in Supplementary Table S2. Nuclei were counterstained with DAPI Fluoromount-G® (Southern Biotech, Birmingham, AL, USA). All stained slides were imaged with Cytation5 (BioTek Instruments Agilent Technologies, USA).

Primary salivary cell isolation and expansion

The cryopreserved tissues were partially thawed in a water bath maintained at 37 °C and retrieved by centrifugation at 300 g for 5 min in HBSS buffer supplemented with 2% FCS and 1x penicillin-streptomycin. Single-cell suspensions were then obtained from tissue-organoids by serially dissociating with trypsin-EDTA (0.25%, STEMCELL Technologies), 5 mg/mL dispase (STEMCELL Technologies), supplemented with 100 μg/mL DNase1 (Sigma-Aldrich). The cell suspension was passed through a 40-μm strainer into a 50 ml centrifuge tube[17].Subsequently, the tubes were centrifuged to pellet the cells and resuspended in appropriate buffered media. Viable cells were counted following trypan blue (0.4%, Gibco) staining in Neuber's chamber and subsequently, cells were 2D cultured in media-1 as described elsewhere[21].

3D-matrigel salivary organoid-initiating cell (OIC) assay and organoid analysis

Freshly dissociated salivary cells from cryopreserved organoids were evaluated for OIC activity in a 3D-matrigel culture as described previously for human mammary cells[21]. In brief, a suspension of 25,000 freshly dissociated cells or culture-expanded/FACS-sorted cells ranging from 625 to 5000 cells were prepared in growth factor reduced Matrigel (R&D Systems) and plated in 96-well plates as domes. The domes were allowed to solidify for 15–30 min. Subsequently, 200 μL of pre-warmed media-1 and media-2 was added. media-1 is prepared using DMEM/F12 (Ham, Gibco), supplemented with 5% FCS, 10 ng/ml EGF, 10 ng/ml cholera toxin (Sigma), 1 μg/ml insulin (Sigma) and 0.5 μg/ml hydrocortisone (Sigma)[21]. Limited studies were carried out using media-2 but was prepared using Advanced DMEM/F12 (Gibco) supplemented with 1% B27, 10 ng/mL EGF, and SB431542 as published elsewhere[77]. The frequency of 3D organoid-initiating cells (OIC) was calculated by dividing the number of organoids formed by the number of cells plated.

2D colony-forming cell (CFC) assay

The culture-expanded or FACS purified salivary cells with distinct phenotypes were seeded at densities of 200, 600 and 1800 in a 6-well plate and cultured for 10 days in media-1. The media was removed and cells were rinsed with PBS, fixed using acetone:methanol (1:3), and then stained with Giemsa stain (Sigma-Aldrich) for colony visualization. Colony morphologies were visualized using microscope and classified into various types as described elsewhere[19,20,40]. The frequency of colony-forming or progenitor cells was calculated by dividing the number of colonies formed by the number of cells plated.

Flow cytometry

Salivary cells from cryopreserved tissue-organoids, cultured 3D-matrigel organoids or 2D culture expanded cells at different passages were analyzed by FACS. In order to isolate cells from organoids, the organoid-matrigel pellet was resuspended in 100 μL of Cell Recovery Solution (Corning) and incubated on ice for 30 min. The solution was centrifuged at 2500 x g for 10 min and the supernatant removed to isolate salivary cells from Matrigel. 500 μL of 0.05% Trypsin was added and the solution was mixed by pipetting up and down. 1 mL of HBSS (Gibco) supplemented with 2% FBS was then added prior to a 5 min incubation at 37 °C and subsequent centrifugation to yield single cells. The cells were stained with anti-human fluorochrome-conjugated antibodies listed in Supplementary Table S3, and DAPI to identify dead (DAPI +) cells. Stained cells were analyzed using FACS-Melody cell sorter/analyzer (BD Biosciences), as described elsewhere[21]. The FCS data files were analyzed using FlowJo data analysis software package. We typically sorted 50,000–200,000 cells in an experiment.

MTT-based cell proliferation assay

The PG cell suspension of passage 1 was prepared and dispensed at density of 2000 cells/well of a 96 well plate in 90 μl of media-1. The plates were incubated at 37 °C, 5% CO_2 for 24 hours. A serial dilution of H_2O_2 ranging from 0 to 1000 μM in DMEM (Gibco) basal media was prepared in a separate 96 well plate. Subsequently, 10 μl of each dilution was transferred respective to wells of plate with cells (0–100 μM) and incubated for 48 hours. Subsequently, 10 μL MTT (5 mg/ml tetrazolium salt 3-[4,5-dimethylthiazol-2-yl]-2,5-diphenyltetrazolium bromide, Sigma-Aldrich) was added to

each well and kept in a dark for 4 h at 37 °C. The MTT crystals were solubilized overnight in solubilization solution (10% SDS in 0.01 N HCl) and absorbance was measured at 570 nm and 660 nm using Cytation 5 plate reader (BioTek)[21].

PSMA gene promoter CpG methylation analysis

DNA samples 1 μg obtained from living SMG tissue underwent bisulfite conversion using the Epitect Bisulfite Kit (Qiagen). Genomic DNA was denatured by sodium hydroxide treatment, followed by bisulfite conversion to selectively modify unmethylated cytosines to uracils, while preserving methylated cytosines. The resulting bisulfite-converted DNA was purified using Epitect spin columns. Desulfonation was carried out to remove sulfonate groups, and after successive washes, the bisulfite-converted DNA was eluted with an appropriate buffer. Primers targeting the PSMA CpG islands from the bisulfite-converted DNA were designed using Meth Primer software[78]. PCR amplification was performed using Q5 high-fidelity polymerase (NEB) to amplify the targeted regions. The resulting amplicons were subjected to Sanger sequencing. Sequencing data were analyzed using the web-based tool QUMA (QUantification tool for Methylation Analysis). QUMA facilitated bisulfite sequencing analysis of CpG methylation, providing essential data-processing functions and ensuring consistent quality control throughout the analysis process[79].

RNA extraction, cDNA synthesis and RT-PCR

Total RNA was extracted from 2D and 3D cell cultures using TRIzol reagent (Thermo Fisher Scientific) according to the manufacturer's protocol. The RNA concentration and purity were determined using a nanophotometer, and 200 ng of RNA was used for cDNA synthesis, using the Superscript III First-Strand Synthesis System (Invitrogen) with random hexamers following the manufacturer's instructions. Gene-specific primers for RT-PCR were designed using the NCBI Primer-BLAST tool (Supplementary Table S4). RT-PCR was performed using the Q5 Hot Start High-Fidelity PCR Master Mix (New England Biolabs). Amplified products were verified by agarose gel electrophoresis.

Salivary single-cell RNA sequencing analysis

Adult C3H Mus musculus SMG single-cell RNA sequencing (scRNA-seq) data (GSM4546898) from Hauser et al.[46] was analyzed in R and R-Studio. Data analysis and visualization were performed using Seurat v5.0.1, tidyverse v2.0.0, and ggplot2 v3.4.4. Cells with fewer than 200 features, less than 1% of UMIs mapping to ribosomal genes, or greater than 10% UMIs mapping to mitochondrial genes were considered non-viable and excluded from analysis. Cells with greater than 2500 features were removed as an extra precaution against cell doublets. Additionally, cells with greater than 0.5% of UMIs mapping to hemoglobin genes were removed from analysis to exclude blood cells. Normalization and scaling were performed following Seurat's default pipeline. 30 PCs from principal component analysis were computed to perform dimensionality reduction for clustering. Cell types were annotated based on protein and gene expression signatures cross-referenced through Human Protein Atlas immunostaining, Mouse Genome Informatics[80], Enrichr[81], Hauser et al. 2020[46], and additional literature review. Murine analogs of human proteins were manually evaluated through cross-referencing Mouse Genome Informatics[80] and HUGO Gene Nomenclature Committee[82] databases.

Sample preparation for salivary single-cell proteomics

Following FACS-based separation of viable progenitor-rich salivary single cells from SMG and PG, cells were sorted, and reactions were performed on a 384-well plate using the cellenONE system (Cellenion, France)[83]. Lysis buffer was prepared with the concentration of 0.2% DDM (324355-1GM, Millipore, USA), 100 mM TEAB (T7408-500ML, Sigma-Aldrich, USA) and 2 ng/μl trypsin protease (90057, Thermo Scientific, USA). Prior to single-cell deposition, 1000 drops (~ 350 nl) of lysis buffer were dispensed into each well of 384-well plate. Single cells were then isolated and deposited into the wells containing lysis buffer. The plate was incubated on the heating deck

inside the cellenONE at 37 °C for 1 h. Digestion was then quenched by adding 300 drops (~100 nl) of 5% formic acid. Digested samples from each well were reconstituted in 4 μl of 0.1% formic acid containing 0.05x iRT peptides (Biognosys, Ki-3002-1). For generation of a spectral library, 20 cells were collected and processed following the same procedures.

Liquid chromatography-tandem mass spectrometry (LC-MS/MS) data acquisition and analysis

Peptide samples were directly injected from the 384-well plate and separated on an analytical column (15 cm x 75 μm, C$_{18}$ 1.7 μm, IonOpticks, AUR3-15075C18-CSI) using nanoElute 2 liquid chromatography system (Bruker Daltonics, Bremen, Germany). Solvent A (0.1% formic acid in water) and solvent B (0.1% formic acid in acetonitrile) were used to generate linear gradient over 38 min using a flow rate of 250 nl/min; 2–27% solvent B in 20 min, 27–40% solvent B in 5 min, 30–60% solvent B in 5 min, maintaining at 60–80% solvent B for 5 min, and 5% solvent B for 5 min. Separated peptides were analyzed using timsTOF SCP mass spectrometer (Bruker Daltonics, Bremen, Germany) in diaPASEF mode[84]. Ions in the range of 400–1000 m/z were monitored with isolation window of 25 m/z and 8 PASEF scans per cycle along with 3 steps per PASEF scan. To generate a spectral library, DDA-PASEF data were acquired with 10 PASEF scans as described previously[44].

The raw mass spectrometry data were analyzed using DIA-NN (version 1.8) using the following settings: protein inference=genes, quantification strategy=Robust LC (high accuracy) and cross-run normalization=global. The DDA-PASEF data from 20 cells were search against the UniProt human protein database (20,430 entries) using MSFragger (version 4.0) embedded in the FragPipe suite (version 21.1). Two missed cleavages were considered with a fully tryptic option. Oxidation of methionine, acetylation of protein N-terminal/lysine, phosphorylation of serine/threonine/tyrosine and methylation, dimethylation and trimethylation of lysine were considered. Batch effect between data of Patient #1 and Patient #2 was corrected using Combat[85] available at https://www.guomics.com/BatchServer/

Statistical analysis

All analyses were performed using GraphPad Prism 8.0. Differences were considered significant at p-value < 0.05. Data is displayed as mean ± SEM unless otherwise stated.

Data availability

The mass spectrometry proteomics data have been deposited to the ProteomeXchange Consortium via the PRIDE[86] partner repository with the dataset identifier PXD055869.

References

1. Chibly, A. M., Aure, M. H., Patel, V. N. & Hoffman, M. P. Salivary gland function, development, and regeneration. *Physiol. Rev.* **102**, 1495–1552 (2022).
2. Pedersen, A. M. L., Sorensen, C. E., Proctor, G. B., Carpenter, G. H. & Ekstrom, J. Salivary secretion in health and disease. *J. Oral. Rehabil.* **45**, 730–746 (2018).
3. Mercadante, V., Al Hamad, A., Lodi, G., Porter, S. & Fedele, S. Interventions for the management of radiotherapy-induced xerostomia and hyposalivation: A systematic review and meta-analysis. *Oral. Oncol.* **66**, 64–74 (2017).
4. Taïeb, D. et al. PSMA-Targeted Radionuclide Therapy and Salivary Gland Toxicity: Why Does It Matter?. *J. Nucl. Med.* **59**, 747–748 (2018).
5. Emperumal, C. P. et al. Oral Toxicities of PSMA-Targeted Immunotherapies for The Management of Prostate Cancer. *Clin. Genitourinary Cancer* **22**, 380–384 (2023).

6. Musheer Aalam, S. M. et al. Characterization of Transgenic NSG-SGM3 Mouse Model of Precision Radiation-Induced Chronic Hyposalivation. *Radiat. Res.* **198**, 243–254 (2022).

7. Kim, J. Y., An, C. H., Kim, J. Y. & Jung, J. K. Experimental Animal Model Systems for Understanding Salivary Secretory Disorders. *Int. J. Mol. Sci.* **21**, 8423 (2020).

8. Maimets, M. et al. Long-Term In Vitro Expansion of Salivary Gland Stem Cells Driven by Wnt Signals. *Stem Cell Rep.* **6**, 150–162 (2016).

9. Pringle, S. et al. Human Salivary Gland Stem Cells Functionally Restore Radiation Damaged Salivary Glands. *Stem Cells* **34**, 640–652 (2016).

10. Lombaert, I. M. et al. Rescue of salivary gland function after stem cell transplantation in irradiated glands. *PLoS One* **3**, e2063 (2008).

11. Makarem, M. et al. Developmental changes in the in vitro activated regenerative activity of primitive mammary epithelial cells. *PLoS Biol.* **11**, e1001630 (2013).

12. Prater, M. D., et al. Mammary stem cells have myoepithelial cell properties. *Nat. Cell Biol.* **16**, 942–950 (2014).

13. Guo, W. et al. Slug and Sox9 cooperatively determine the mammary stem cell state. *Cell* **148**, 1015–1028 (2012).

14. Aure, M. H., Konieczny, S. F. & Ovitt, C. E. Salivary gland homeostasis is maintained through acinar cell self-duplication. *Dev. Cell* **33**, 231–237 (2015).

15. May, A. J. et al. Diverse progenitor cells preserve salivary gland ductal architecture after radiation-induced damage. *Development* **145**, dev166363 (2018).

16. He, Z. et al. Pathogenic BRCA1 variants disrupt PLK1-regulation of mitotic spindle orientation. *Nat. Commun.* **13**, 2200 (2022).

17. Eirew, P. et al. A method for quantifying normal human mammary epithelial stem cells with in vivo regenerative ability. *Nat. Med.* **14**, 1384–1389 (2008).

18. Stingl, J., Eaves, C. J., Zandieh, I. & Emerman, J. T. Characterization of bipotent mammary epithelial progenitor cells in normal adult human breast tissue. *Breast Cancer Res Treat.* **67**, 93–109 (2001).

19. Raouf, A. et al. Transcriptome analysis of the normal human mammary cell commitment and differentiation process. *Cell Stem Cell* **3**, 109–118 (2008).

20. Kannan, N. et al. The luminal progenitor compartment of the normal human mammary gland constitutes a unique site of telomere dysfunction. *Stem Cell Rep.* **1**, 28–37 (2013).

21. Kannan, N. et al. Glutathione-dependent and -independent oxidative stress-control mechanisms distinguish normal human mammary epithelial cell subsets. *Proc. Natl Acad. Sci. USA* **111**, 7789–7794 (2014).

22. Eirew, P. et al. Aldehyde dehydrogenase activity is a biomarker of primitive normal human mammary luminal cells. *Stem Cells* **30**, 344–348 (2012).

23. Chakrabarti, R., et al. ΔNp63 promotes stem cell activity in mammary gland development and basal-like breast cancer by enhancing Fzd7 expression and Wnt signalling. *Nat. Cell Biol.* **16**, 1004–1015 (2014).

24. Nguyen, L. V. et al. Clonal analysis via barcoding reveals diverse growth and differentiation of transplanted mouse and human mammary stem cells. *Cell Stem Cell* **14**, 253–263 (2014).

25. Joshi, P. A. et al. RANK Signaling Amplifies WNT-Responsive Mammary Progenitors through R-SPONDIN1. *Stem Cell Rep.* **5**, 31–44 (2015).

26. Pellacani, D. et al. Analysis of Normal Human Mammary Epigenomes Reveals Cell-Specific Active Enhancer States and Associated Transcription Factor Networks. *Cell Rep.* **17**, 2060–2074 (2016).

27. Knapp, D., Kannan, N., Pellacani, D. & Eaves, C. J. Mass Cytometric Analysis Reveals Viable Activated Caspase-3(+) Luminal Progenitors in the Normal Adult Human Mammary Gland. *Cell Rep.* **21**, 1116–1126 (2017).

28. Mahendralingam, M. J. et al. Mammary epithelial cells have lineage-rooted metabolic identities. *Nat. Metab.* **3**, 665–681 (2021).

29. Mateo, F. et al. Modification of BRCA1-associated breast cancer risk by HMMR overexpression. *Nat. Commun.* **13**, 1895 (2022).

30. Kim, H. et al. Differential DNA damage repair and PARP inhibitor vulnerability of the mammary epithelial lineages. *Cell Rep.* **42**, 113256 (2023).

31. Clevers, H. Modeling Development and Disease with Organoids. *Cell* **165**, 1586–1597 (2016).

32. Tanaka, J. et al. Human induced pluripotent stem cell-derived salivary gland organoids model SARS-CoV-2 infection and replication. *Nat. Cell Biol.* **24**, 1595–1605 (2022).

33. Yoon, Y. J. et al. Salivary gland organoid culture maintains distinct glandular properties of murine and human major salivary glands. *Nat. Commun.* **13**, 3291 (2022).

34. Lim, E. et al. Aberrant luminal progenitors as the candidate target population for basal tumor development in BRCA1 mutation carriers. *Nat. Med.* **15**, 907–913 (2009).

35. Nanduri, L. S. et al. Purification and ex vivo expansion of fully functional salivary gland stem cells. *Stem Cell Rep.* **3**, 957–964 (2014).

36. David, R., Shai, E., Aframian, D. J. & Palmon, A. Isolation and cultivation of integrin alpha(6)beta(1)-expressing salivary gland graft cells: a model for use with an artificial salivary gland. *Tissue Eng. Part A* **14**, 331–337 (2008).

37. Heynickx, N., Herrmann, K., Vermeulen, K., Baatout, S. & Aerts, A. The salivary glands as a dose limiting organ of PSMA- targeted radionuclide therapy: A review of the lessons learnt so far. *Nucl. Med Biol.* **98-99**, 30–39 (2021).

38. Meirovitz, A. et al. The potential of somatostatin receptor 2 as a novel therapeutic target in salivary gland malignant tumors. *J. Cancer Res Clin. Oncol.* **147**, 1335–1340 (2021).

39. Chatterjee, S., Basak, P., Buchel, E., Murphy, L. C. & Raouf, A. A robust cell culture system for large scale feeder cell-free expansion of human breast epithelial progenitors. *Stem Cell Res Ther.* **9**, 264 (2018).

40. Azuma, M., Tamatani, T., Kasai, Y. & Sato, M. Immortalization of normal human salivary gland cells with duct-, myoepithelial-, acinar-, or squamous phenotype by transfection with SV40 ori- mutant deoxyribonucleic acid. *Lab Invest* **69**, 24–42 (1993).

41. Byrne, H. Three-dimensional biological cultures and organoids. *Interface Focus* **10**, 20200014 (2020).

42. Meier, F. et al. Online Parallel Accumulation-Serial Fragmentation (PASEF) with a Novel Trapped Ion Mobility Mass Spectrometer. *Mol. Cell Proteom.* **17**, 2534–2545 (2018).

43. Brunner, A. D. et al. Ultra-high sensitivity mass spectrometry quantifies single-cell proteome changes upon perturbation. *Mol. Syst. Biol.* **18**, e10798 (2022).

44. Mun, D. G. et al. Diversity of post-translational modifications and cell signaling revealed by single cell and single organelle mass spectrometry. *Commun. Biol.* **7**, 884 (2024).

45. Sanz-Gomez, N., Freije, A. & Gandarillas, A. Keratinocyte Differentiation by Flow Cytometry. *Methods Mol. Biol.* **2109**, 83–92 (2020).

46. Hauser, B. R. et al. Generation of a Single-Cell RNAseq Atlas of Murine Salivary Gland Development. *iScience* **23**, 101838 (2020).

47. Horeth, E. et al. High-Resolution Transcriptomic Landscape of the Human Submandibular Gland. *J. Dent. Res.* **102**, 525–535 (2023).

48. Fu, N. Y. et al. Identification of quiescent and spatially restricted mammary stem cells that are hormone responsive. *Nat. Cell Biol.* **19**, 164–176 (2017).

49. Perkins, A., Nelson, K. J., Parsonage, D., Poole, L. B. & Karplus, P. A. Peroxiredoxins: guardians against oxidative stress and modulators of peroxide signaling. *Trends Biochem Sci.* **40**, 435–445 (2015).

50. Tothova, L., Kamodyova, N., Cervenka, T. & Celec, P. Salivary markers of oxidative stress in oral diseases. *Front Cell Infect. Microbiol* **5**, 73 (2015).

51. Boahene, D. K. et al. Mucoepidermoid carcinoma of the parotid gland: the Mayo clinic experience. *Arch. Otolaryngol. Head. Neck Surg.* **130**, 849–856 (2004).

52. Devaraju, R., Gantala, R., Aitha, H. & Gotoor, S. G. Mucoepidermoid carcinoma. *BMJ Case Rep.* **2014**, bcr-2013–202776 (2014).

53. Quer, M. et al. Current Trends and Controversies in the Management of Warthin Tumor of the Parotid Gland. *Diagnostics (Basel)* **11**, 1467 (2021).

54. Matuck, B. F. et al. Salivary glands are a target for SARS-CoV-2: a source for saliva contamination. *J. Pathol.* **254**, 239–243 (2021).

55. Huang, N. et al. SARS-CoV-2 infection of the oral cavity and saliva. *Nat. Med.* **27**, 892–903 (2021).

56. Farag, A. M., Holliday, C., Cimmino, J., Roomian, T. & Papas, A. Comparing the effectiveness and adverse effects of pilocarpine and cevimeline in patients with hyposalivation. *Oral. Dis.* **25**, 1937–1944 (2019).

57. See, L., Mohammadi, M., Han, P. P., Mulligan, R. & Enciso, R. Efficacy of saliva substitutes and stimulants in the treatment of dry mouth. *Spec. Care Dent.* **39**, 287–297 (2019).

58. Lai, Z. et al. Aquaporin gene therapy corrects Sjogren's syndrome phenotype in mice. *Proc. Natl Acad. Sci. USA* **113**, 5694–5699 (2016).

59. Nakamura, H. et al. Correction of LAMP3-associated salivary gland hypofunction by aquaporin gene therapy. *Sci. Rep.* **12**, 18570 (2022).

60. Marinkovic, M. et al. Extracellular matrix turnover in salivary gland disorders and regenerative therapies: Obstacles and opportunities. *J. Oral. Biol. Craniofac Res.* **13**, 693–703 (2023).

61. van Luijk, P. et al. Sparing the region of the salivary gland containing stem cells preserves saliva production after radiotherapy for head and neck cancer. *Sci. Transl. Med.* **7**, 305ra147 (2015).

62. Rocchi, C., Barazzuol, L. & Coppes, R. P. The evolving definition of salivary gland stem cells. *NPJ Regen. Med.* **6**, 4 (2021).

63. Emmerson, E. & Knox, S. M. Salivary gland stem cells: A review of development, regeneration and cancer. *Genesis* **56**, e23211 (2018).

64. Xiao, N. et al. Neurotrophic factor GDNF promotes survival of salivary stem cells. *J. Clin. Invest* **124**, 3364–3377 (2014).

65. Nanduri, L. S. et al. Regeneration of irradiated salivary glands with stem cell marker expressing cells. *Radiother. Oncol.* **99**, 367–372 (2011).

66. Nanduri, L. S. et al. Salisphere derived c-Kit+ cell transplantation restores tissue homeostasis in irradiated salivary gland. *Radiother. Oncol.* **108**, 458–463 (2013).

67. Yoon, S. M. et al. Epithelial cell adhesion molecule (EpCAM) marks hepatocytes newly derived from stem/progenitor cells in humans. *Hepatology* **53**, 964–973 (2011).

68. Stingl, J., Raouf, A., Eirew, P. & Eaves, C. J. Deciphering the mammary epithelial cell hierarchy. *Cell Cycle* **5**, 1519–1522 (2006).

69. Uhlen, M. et al. Proteomics. Tissue-based map of the human proteome. *Science* **347**, 1260419 (2015).

70. Perner, S. et al. Prostate-specific membrane antigen expression as a predictor of prostate cancer progression. *Hum. Pathol.* **38**, 696–701 (2007).

71. Kinoshita, Y. et al. Expression of prostate-specific membrane antigen in normal and malignant human tissues. *World J. Surg.* **30**, 628–636 (2006).

72. Carter, R. E., Feldman, A. R. & Coyle, J. T. Prostate-specific membrane antigen is a hydrolase with substrate and pharmacologic characteristics of a neuropeptidase. *Proc. Natl Acad. Sci. USA* **93**, 749–753 (1996).

73. Knox, S. M. et al. Parasympathetic innervation maintains epithelial progenitor cells during salivary organogenesis. *Science* **329**, 1645–1647 (2010).

74. Lombaert, I. M., Knox, S. M. & Hoffman, M. P. Salivary gland progenitor cell biology provides a rationale for therapeutic salivary gland regeneration. *Oral. Dis.* **17**, 445–449 (2011).

75. Zhang, S. et al. Derivation of Human Salivary Epithelial Progenitors from Pluripotent Stem Cells via Activation of RA and Wnt Signaling. *Stem Cell Rev. Rep.* **19**, 430–442 (2023).

76. Yu, S. et al. Loss of ATG5 in KRT14(+) cells leads to accumulated functional impairments of salivary glands via pyroptosis. *FASEB J.* **36**, e22631 (2022).

77. Feng, L. et al. Protocol for the Detection of Organoid-Initiating Cell Activity in Patient-Derived Single Fallopian Tube Epithelial Cells. *Methods Mol. Biol.* **2429**, 445–454 (2022).

78. Li, L. C. & Dahiya, R. MethPrimer: designing primers for methylation PCRs. *Bioinformatics* **18**, 1427–1431 (2002).

79. Kumaki, Y., Oda, M. & Okano, M. QUMA: quantification tool for methylation analysis. *Nucleic Acids Res.* **36**, W170–W175 (2008).

80. Bult, C. J. et al. Mouse Genome Database (MGD) 2019. *Nucleic Acids Res.* **47**, D801–D806 (2019).

81. Chen, E. Y. et al. Enrichr: interactive and collaborative HTML5 gene list enrichment analysis tool. *BMC Bioinforma.* **14**, 128 (2013).

82. Seal, R. L. et al. Genenames.org: the HGNC resources in 2023. *Nucleic Acids Res.* **51**, D1003–D1009 (2023).

83. Mun, D. G. et al. Optimizing single cell proteomics using trapped ion mobility spectrometry for label-free experiments. *Analyst* **148**, 3466–3475 (2023).

84. Meier, F. et al. diaPASEF: parallel accumulation-serial fragmentation combined with data-independent acquisition. *Nat. Methods* **17**, 1229–1236 (2020).

85. Zhu, T. et al. BatchServer: A Web Server for Batch Effect Evaluation, Visualization, and Correction. *J. Proteome Res.* **20**, 1079–1086 (2021).

86. Perez-Riverol, Y. et al. The PRIDE database resources in 2022: a hub for mass spectrometry-based proteomics evidences. *Nucleic Acids Res.* **50**, D543–D552 (2022).

Acknowledgements

Author contributions

M.A., A.R.V., A.K., R.M., and C.P.E. contributed to biobanking, data collection and analysis and preparation of the manuscript draft. D.G.M. and A.P. contributed to mass spectrometry data and analysis. R.C. and I.L. critically reviewed and assisted with manuscript preparation. J.J. and N.K. funded the study. N.K. conceptualized, designed and supervised the study and finalized the manuscript. All authors contributed to the drafting of the manuscript.

Competing interests

The authors declare no competing interests.

Additional information

Supplementary information The online version contains supplementary material available at https://doi.org/10.1038/s41536-025-00410-5.

Correspondence and requests for materials should be addressed to Jeffrey R. Janus or Nagarajan Kannan.

Reprints and permissions information is available at http://www.nature.com/reprints

Publisher's note Springer Nature remains neutral with regard to jurisdictional claims in published maps and institutional affiliations.